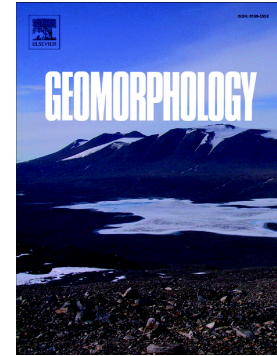


Accepted Manuscript

Quaternary regional evolution based on karst cave geomorphology in Picos de Europa (Atlantic Margin of the Iberian Peninsula)

Daniel Ballesteros, Santiago Giralt, Joaquín García-Sansegundo, Montserrat Jiménez-Sánchez



PII: S0169-555X(19)30142-4
DOI: <https://doi.org/10.1016/j.geomorph.2019.04.002>
Reference: GEOMOR 6730
To appear in: *Geomorphology*
Received date: 26 June 2018
Revised date: 13 February 2019
Accepted date: 1 April 2019

Please cite this article as: D. Ballesteros, S. Giralt, J. García-Sansegundo, et al., Quaternary regional evolution based on karst cave geomorphology in Picos de Europa (Atlantic Margin of the Iberian Peninsula), *Geomorphology*, <https://doi.org/10.1016/j.geomorph.2019.04.002>

This is a PDF file of an unedited manuscript that has been accepted for publication. As a service to our customers we are providing this early version of the manuscript. The manuscript will undergo copyediting, typesetting, and review of the resulting proof before it is published in its final form. Please note that during the production process errors may be discovered which could affect the content, and all legal disclaimers that apply to the journal pertain.

Quaternary regional evolution based on karst cave geomorphology in Picos de Europa (Atlantic Margin of the Iberian Peninsula)

Daniel Ballesteros (1), Santiago Giralt (2), Joaquín García-Sansegundo (3), Montserrat Jiménez-Sánchez (3).

1 UMR 6266 IDEES, University of Rouen Normandy-CNRS, Mont Saint-Aignan CEDEX, France. ballesteros@geol.uniovi.es

2 Earth Sciences Institut Jaume Almera (CSIC), c/Lluís Solé i Sabarís s/n 08028 Barcelona, Spain. sgiralt@ictja.csic.es

3 Department of Geology, University of Oviedo, c/ Jesús Arias de Velasco s/n 33005 Oviedo, Spain. J.g.sansegundo@geol.uniovi.es, mjimenez@geol.uniovi.es

Abstract

Alpine caves have attracted considerable geomorphological, paleoenvironmental and hydrogeological interest since climate, glaciations, relief uplift, fluvial incision and karst aquifer control their evolution. In the Atlantic Margin of the Iberian Peninsula, Picos de Europa mountains is among of the most important karst areas of the World containing some of the deepest caves explored today. In addition, these mountains represent a reference site for the study of the Last Glacial Cycle in the SW of Europe. This work aims to reconstruct the Pliocene-Quaternary evolution of this region based on geomorphological and geochronological research (U/Th and Al/Be) carried out in four alpine caves. Cave geomorphological mapping evidences that 12 km of studied caves are made up of 47 % vadose canyons and shafts, 45 % phreatic/epiphreatic conduits organised in six cave levels, and 7 % breakdown-modified passages. Their deposits are characterized by speleothems, including flowstones, that represent ancient cave pavements, fluvial terrace deposits with allochthonous clasts, slackwater deposits related to cave floods, and debris deposits produced by breakdown. One $^{26}\text{Al}/^{10}\text{Be}$ burial age indicates a minimum age of 2.1 ± 0.5 Ma for the caves origin, allowing

estimation of the mountain uplift at $0.15\text{--}0.25\text{ mm a}^{-1}$ since the Late Pliocene. Twenty-eight new $^{234}\text{U}/^{230}\text{Th}$ ages and another six previous speleothem ages give ages ranging from MIS 8 to 1. The speleogenetic model comprises six phases of regional evolution. Phase 1: main development of cave levels with SE-directed phreatic flow in the NW of Picos de Europa, in a karst partially or totally covered by the detrital Permian-Mesozoic cover, presently eroded. Phase 2: erosion of the Permian-Mesozoic cover and onset of vadose conditions before 260 ka, in a karst-affected by fluvial captures. Phase 3: cave infill during 220–145 ka, probably caused by the erosion of Stephanian detrital outcrops. Phase 4: erosion of cave infill during 125–45 ka. Phase 5: apparent pause in the speleothem formation during 45–25 ka related to dry and cold regional conditions. Phase 6: reactivation of the speleothem precipitation since 25 ka. Regional climate, fluvial incision and the ancient presence of detrital outcrops at the surface appear to have been the main factors that controlled the cave evolution and regional geomorphological evolution throughout Pliocene and Quaternary times.

Keywords: alpine karst, geomorphology, geochronology, speleogenesis.

1. Introduction

Alpine caves are dominated by successions of vadose canyons and shafts developed in mountain karst areas (Maire, 1990), which correspond frequently to glaciokarsts (Ford, 1987). Alpine caves are of interest as they are developed close to the zero degrees isotherm. This makes them very sensitive to climatic and environmental change (Johnston et al., 2013; Luetscher et al., 2015). In these areas, low temperatures limit the vegetation productivity, reducing soil pCO_2 , acid organics and drip water saturation (Lauritzen and Skoglund, 2013; Zhou et al., 2015). Alpine caves support important speleothems and ice records in glaciated areas of South Europe

during the Quaternary, such as the Alps and Pyrenees (Miorandi et al., 2010; Wackerbarth et al., 2012; Weremeichik and Mylroie, 2014). Further, the presence of remains of troglobitic/stygobitic fauna in alpine caves indicates past climate fluctuations and glacial ice extensions (Eme et al., 2014).

The study of the geometry and deposits of alpine caves reveals valuable information about glaciations, fluvial evolution, relief uplift and neotectonics over the past several millions of years (Audra et al., 2006; De Waele and Pasini, 2013). Regarding cave geometry, alpine cavities usually show several cave levels formed by phreatic and epiphreatic conducts originated at the water table (Palmer, 1987). Thus, cave levels represent ancient water tables that can be currently located 1-2 km above the saturated zone of karst aquifer (e.g. Plan et al., 2009; Calvet et al., 2015). This situation evidences the lowering of the water table, triggered by fluvial incision caused by mountain uplift or the drop of the fluvial base level, which is frequently related to glacier stages (Audra et al., 2006). Regarding cave deposits, they constitute exceptional records preserved over long timescales. In lowland areas, surficial deposits are well preserved and can be useful for reconstructing the geomorphological and climatic evolution of a region. However, in upland areas where erosion has removed much of the surface evidence, cave deposits represent the most common and best-preserved archive of palaeoenvironmental and paleoclimate data. Among these deposits, fluvial deposits came from erosion of the limestone bedrock as well as detrital rocks that cropped out on the surface, thus these sediments constitute evidence of the ancient landscape that was strongly eroded by the last glaciation (Häuselmann, 2013). The dating of cave deposits provides a chronology for the aforementioned cave levels, usually based on minima ages, and the timing of palaeoenvironmental and paleoclimate changes. The $^{234}\text{U}/^{230}\text{Th}$ method is frequently used to date cave deposits up to Middle Pleistocene in age (e.g. Fairchild et al., 2010; Wackerbarth et al., 2012), whereas cave ages obtained by cosmogenic isotopes, U/Pb or paleomagnetism

methods can extend to the Pliocene (e.g. Hobléa et al., 2011; Calvet et al., 2015; Rossi et al., 2016).

Geomorphological studies have shown that alpine karst are probably of Miocene age, and have been strongly modified by later fluvial modifications and Quaternary glaciations (Audra et al., 2002, 2006; Hobléa et al., 2011; Columbu et al., 2015). Flowstone formation usually occurred during warm environmental conditions while detrital sedimentation took place during glacial periods in the Alps (Europe) and Canadian Rocky Mountains, in North America (Ford, 1993; Plan et al., 2009). Therefore, these sediments constitute records of glacial timing, including glacier advances and retreats. Combining absolute dating and geomorphological studies, alpine caves allow the estimation of uplift since the Pliocene, including phases of abrupt valley over-deepening, as the abrupt glacial valley incision occurred at 0.8 Ma in the Alps (Häuselmann et al., 2007), or Quaternary fluvial incision acceleration in the Pyrenees (Calvet et al., 2015). These works also quantified fluvial incision rates, with ranges of 0.1-0.8 mm a⁻¹ for the Quaternary, based on the presence of ancient phreatic conduits perched hundreds of meters above the current watertable. Locally, the study of alpine caves reveals sea-level changes. Alpine caves also hold evidence the timing and deformation mechanism of neotectonic movements based on speleothem damage and displacements in karst conduits, as reported in caves of the Austrian Alps (Plan et al., 2010).

The study of alpine caves reveals data about the geometry and functioning of many karst aquifers that contain significant water resources (Goldscheider and Neukum, 2010; Vigna and Banzato, 2015). These data include variations in phreatic paleoflows directions and paleoaquifer recharge that has occurred since the Miocene (Audra et al., 2002, 2006; Plan et al., 2009).

In spite of their great interest, few alpine caves have been studied in the European Atlantic Margin, with few examples from Scandinavian (North Europe). In SW Europe

(Fig. 1), studies focused on geomorphology, drip water chemistry and speleothems of alpine caves were performed in the Western Pyrenees (Quinif and Maire, 1998) and its extension to the W: the Cantabrian Mountains (Aranburu et al., 2014; Gázquez et al., 2014; Ballesteros et al., 2015a, 2017; Rossi and Lozano, 2016; Rossi et al., 2016).

This work aims to establish the Quaternary geomorphological evolution of Picos de Europa and the influence of the climate and surficial processes (glaciations and others) on its speleogenesis. With this purpose, we combined previous geomorphological and geochronological data of two alpine caves (Ballesteros et al., 2011b, 2015a, 2017) and geomorphological evidence collected in other two cavities, as well as 28 new numerical ages based on $^{234}\text{U}/^{230}\text{Th}$ series dating and one $^{26}\text{Al}/^{10}\text{Be}$ burial age. The length of studied caves reaches 12 km of conduits that represent 3% of the total conduits of Picos de Europa.

2. Setting

Picos de Europa (43.2°N, 4.8°W) is a discrete mountainous area up to 2648 m in elevation and covering 700 km², forming part of the Cantabrian Mountain range (Fig. 1c). Picos de Europa has an Atlantic maritime climate with 1000-1800 mm of precipitation distributed evenly through the year. Average air temperatures range from -3 to 17°C. Above 1500 m altitude, snow cover is present 6-9 months a year.

In general, Carboniferous limestone forms the bedrock although minor Ordovician and Stephanian (~Kasimovian) sandstone and shale crop out in Picos de Europa, mainly along its borders (Bahamonde et al., 2007; Sanz-López et al., 2018). Variscan thrusting affected these rocks in the upper Carboniferous, followed by the Permian-Mesozoic extension faulting, when red sand and silt and other sediments covered the karstified Carboniferous limestone (Merino-Tomé et al., 2009). During these times, Cretaceous hydrothermal activity produced local dolomitization and sulphide mineralization (Symons et al., 2015). Finally, the Alpine orogeny (Paleocene-Miocene) led to the uplift

of the entire Cantabrian Mountains (Fillon et al., 2016; Gallastegui et al., 2016). This uplift caused the erosion of the Permian-Mesozoic cover. A few remnant outcrops of this Permian-Mesozoic cover are preserved in some low-lying areas.

Carboniferous limestone forms a karst aquifer extending over 883 km² but compartmentalised by Ordovician and Stephanian sandstones and shales that represent aquitards, resulting in a dammed karst configuration (Ballesteros et al., 2015d). The saturated zones of the aquifer have less than 200-300 m thickness and unsaturated zones achieve 2.3 km in thickness in some areas. The water tables are placed at 800-1500 m altitude in the S and at 145 m elevation the N of Picos de Europa.

Picos de Europa is divided into three massifs - Eastern, Western and Central - by rivers that formed fluvial canyons up to 2 km deep. Three rivers (the Sella, Cares and Dobra rivers) are consequent courses and flow S to N, forming the regional base-level at 100-200 m altitude. Subsequent rivers (as the Casaño River, Fig. 1c) start in karst springs flowing to the NW or SE constrained by the regional geological structure.

More than 410 km of cave passage have been discovered by speleological groups, including 69 cavities with more than 500 m depth (Fig. 1b). The majority of the deep caves comprise sequences of vadose canyons and shafts, the deepest of which is 1600 m depth (Erra et al., 1999). Sequences of vadose canyons and shafts constitute the majority of the deep caves, reaching 1.6 km of vertical range in the deepest cavity (Erra et al., 1999). Furthermore, ~160 km of phreatic/epiphreatic galleries form at least 24 cave levels developed from 140 to 2400 m altitude, now abandoned by base level lowering and valley incision (Ballesteros et al., 2015b). Smart (1986), Senior (1987) and Fernández-Gibert et al. (2000) proposed a cave evolution which started in the Pliocene when the Permian-Mesozoic rocks still covered Carboniferous limestone. Later, the rivers fitted in the landscape, reaching the Paleozoic bedrock by eroding almost completely the Permian-Mesozoic cover. This situation triggered fluvial valley

deepening and the lowering of local water tables, creating a thick vadose zone with canyons and shafts (vertical conduits) up to 300 m deep, as well as the development of lower cave levels. Locally, Senior (1987) recognized paragenetic features related to alluvial sediments in the upper part of few deep caves.

Glacial ice covered up to 180-195 km² of the extension of Picos de Europa during periods of the Middle and Upper Pleistocene (Villa et al., 2013; Serrano et al., 2016). The glaciers descended up to 600-800 m altitude during the local maximum extension that took place before 46-35 ka (Serrano et al., 2012; Jiménez-Sánchez et al., 2013; Ruiz-Fernández et al., 2016a). During the Upper Pleistocene, glacial advances occurred at 48-35 ka (Serrano et al., 2016), followed by a general retreat under dry and cold conditions. An equilibrium or advance glacial stage took place at ca 23-19 ka, during a wetter period coeval with the Last Glacial Maximum (LGM) (Rodríguez-Rodríguez et al., 2014; Ruiz-Fernández et al., 2016a). The timing of the Last Deglaciation in Picos de Europa would have occurred coevally with the nearby Monasterio Valley (Fig. 1), where glaciers retreated at 18.1-16.7 ka (Rodríguez-Rodríguez et al., 2017). Later, temperature and precipitation increases led to the development of glacial cirques at the end of MIS 2 (Ruiz-Fernández et al., 2016b) and deciduous forest up to 1500 m altitude in the Holocene, although minor glacial advances happened during the Little Ice Age (LIA) (González-Trueba et al., 2008; Moreno et al., 2011). Periglacial conditions affected areas above the 1000 m in elevation, at least between 37 and 29 ka (Nieuwendam et al., 2015). Nowadays, periglacial and snow processes affect the highest areas (Ruiz-Fernández et al., 2016b), with permafrost restricted to ice caves (Berenguer-Sempere et al., 2014).

3. Methodology

The methodology comprises the characterization of the pilot caves' geomorphology and geochronology as well as the geomorphology of the surrounding area (Ballesteros

et al., 2011b, 2015a). All data have been integrated and handled using a Geographic Information System (GIS).

We selected four study pilot caves named Torca Teyera, Torca La Texa, El Frailín de Camplengu, and Pozu Lluçia, which are located at the N of the Western Massif, with entrances placed from 1266 to 1356 m altitude (Fig. 1c). We chose these cavities based on their accessibility and presence of phreatic/epiphreatic galleries between 800 and 1500 m a.s.l., at the same altitudes of the main cave levels of Picos de Europa (Ballesteros et al., 2015b).

We undertook speleological, geomorphological and geochronological analyses for each pilot cave. We constructed geomorphological maps for these caves at a 1:200 scale, representing the cave features and deposits on the speleological cave survey, elaborated previously according to the UISv1 5-2-BCEF grade defined by Häuselmann (2011). These geomorphological maps depicted the spatial and relative-temporal distribution of the cave forms, and allowed us to identify the type of conduit according to its origin. The addition of the length of each type of conduit provides the percentage of the caves formed by each conduit. Finally, we defined the cave levels combining the mapped phreatic evidences and vertical distribution of cave conduits following Ballesteros et al. (2015a).

The construction of a robust chronological framework for these five studied caves required 28 new $^{234}\text{U}/^{230}\text{Th}$ speleothem dates and one new $^{26}\text{Al}/^{10}\text{Be}$ burial age in a fluvial deposit. Prior to the radiometric dating, we analysed the petrographic texture the speleothems using optical microscopy in order to exclude speleothems that presented corrosion or crystals with irregular limits between minerals. We applied the U/Th disequilibria method by alpha-spectrometry from the Institute of Earth Sciences Jaume Almera (ICTJA-CSIC, Barcelona, Spain). We undertook chemical separation of the radioisotopes and purification from a speleothem sample (~20 g) following the procedure described by Bischoff et al. (1988), and isotope electrodeposition was done

according to the method of Talvitie (1972), modified by Hallstadius (1984). We counted isotope concentrations using an ORTEC OCTETE PLUS spectrometer equipped with eight BR-024-450-100 detectors of Ivanovich and Harmon (1992) and calculated the absolute ages employing the software designed by Rosenbauer (1991). We applied the isochron method (Bischoff and Fitzpatrick, 1991) to date five samples with ~2-5% wt of detrital residue. In all cases, we evaluated the possible detrital contamination of the dated speleothems based on the $^{230}\text{Th}/^{232}\text{Th}$ ratio (Bischoff and Fitzpatrick, 1991), which evaluates the relation between the concentration of ^{230}Th (with radiogenic and detrital origin) and ^{232}Th (with only detrital origin). A $^{230}\text{Th}/^{232}\text{Th}$ ratio (see later, Table 2) higher than one or two indicates that detrital contamination is not significant.

We obtained a single cosmogenic burial age for a fluvial sediment from Torca Teyera cave based on the determination of $^{10}\text{Be}/^9\text{Be}$ and $^{26}\text{Al}/^{27}\text{Al}$ ratios by the Purdue Rare Isotope Measurement Laboratory (Indiana, USA) using an accelerator mass spectrometry. Laboratory procedures include purification of quartz grain from a sand sample (17.379 g), ^{10}Be decontamination, and acid dissolution in HF following Granger et al. (2001). We added also a carrier (303.4 μg) of ^{10}Be . Detect limits of ^9Be and ^{27}Al are 10^{-15} and $5 \cdot 10^{-15}$ of the radionuclides atoms ratios, respectively. We considered 1.02 ± 0.04 for radioactive ^{26}Al mean life and 1.36 ± 0.07 Ma for the ^{10}Be (Chmeleff et al., 2010), estimating the local production rates of the cosmogenic isotopes for 43.27°N latitude and an elevation of 2 km following Stone (2000): $P_{^{10}\text{Al}}=21.50 \text{ at}\cdot\text{g}^{-1}\cdot\text{a}^{-1}$; $P_{^{26}\text{Al}}=145.96 \text{ at}\cdot\text{g}^{-1}\cdot\text{a}^{-1}$. Fraction spallation production is 0.97 and 0.98 for ^{10}Be and ^{26}Al and penetration length neutrons 60 cm (Granger et al., 2007). Analytical uncertainties (reported as 1σ) are based on Arnold et al. (2010).

Finally, we determined the detailed geomorphological context of the selected caves to establish the relationship between cave development and surface evolution. For this, we projected the pilot caves and 144 km of cave conduits on a geomorphological map

of the study area (117 km² in extension), derived from fieldwork, photointerpretation and a GIS analyses.

4. Results

4.1 Cave conduits

Fig. 2 shows the geomorphological maps of the El Frailín de Camplengu and Pozu Lluvia caves, complemented by the published geomorphological maps of the Torca Teyera and Torca La Texa caves (Ballesteros et al., 2011b, 2015a). Table 1 indicates the percentage of conduit type for each of the pilot caves, as well as the altitude of the defined cave levels. The longitude and vertical range of the pilot caves ranges from 2.3 to 4.4 km and 215 to 738 m, respectively. From a genetic point of view, the set of cave conduits includes vadose canyons and shafts, relict phreatic/epiphreatic conduits and breakdown-modified passages.

Vadose canyons and shafts represent 47% of the entire studied caves, varying from 49 to 55% in each cavity. Canyons are usually associated with stepped shafts, although independent shafts up to 80 m high are also recognized in the pilot caves. The incision and the horizontal migration of cave streams (Fig. 4a) developed vadose canyons, invasion canyons and independent shafts, which intercepted previous phreatic/epiphreatic conduits or fed into them. The canyons show pendants and corrosion notches that appear associated with alluvial deposits, thus the origin of these erosive features is paragenetic according to Farrant et al. (2011).

45% of the pilot caves display phreatic/epiphreatic conduits that represent between 38 and 49% of each cavity. The phreatic/epiphreatic conduits show loops (2-15 m in amplitude) and orientations toward the N in the Torca Teyera cave, and toward the SW in the remaining cavities (Fig. 2). These orientations agree with the scallops and the convergence between different phreatic conduits. Consequently, the phreatic groundwater flowed to the SW, locally to the N in Torca Teyera, during the formation of

these phreatic/epiphreatic conduits. Dissolution cupolas, phreatic/epiphreatic tubes and other phreatic features (Figs. 3, 4a) provide evidence the presence of six cave levels at 1300, 1240-1270, 1150-1190, 1080, 700-800 and 615 m a.s.l. (Fig. 3; Table 1). Cave level 1 only appears in the Torca Teyera cave, whereas levels 2 and 3 form part of the remaining caves. Level 4 can be identified in the El Frailín de Camplengu and Pozu Llučia caves while levels 5 and 6 are only seen in the Torca Teyera cave.

The studied caves include 7% of breakdown-modified passages, ranging from 5 to 9% depending on the cavity. These passages are previous vadose and phreatic passages modified by breakdown processes that produced the accumulation debris, involving boulders up to 15 m diameter (Fig. 4c).

4.2 Cave deposits

The geomorphological maps of the pilot caves show that speleothems, fluvial, slackwater and debris deposits occupy 68% of the studied cavities (Fig. 2). Fluvial sediments include current thalweg and terrace deposits mainly formed by rounded limestone cobbles and pebbles, with a matrix dominated by quartz and carbonate sand (Fig. 5). Locally, these deposits contain clasts of sandstone, igneous rocks, bauxite, nodules of siderite/limonite and fragments of speleothem. The present stream channels contain thalweg deposits often capped by flowstones that are now being eroded by stream action (Fig. 4a). Fluvial terrace deposits are perched up to 25 m above the bottom of the canyons and phreatic/epiphreatic conduits. Frequently, these deposits are associated with pendants and involve interlayered flowstones very rich in detrital minerals.

Speleothems are frequently flowstones and stalactites precipitated at the walls or above fluvial, slackwater and debris deposits (Figs. 3, 4), and comprise up to 60% of insoluble residue, frequently quartz and clays according to microscope observations. Flowstones show erosive features and form ledges perched up to 10 m above the cave

floor (Fig. 5a). The base of these ledges englobes rounded pebbles, thus these flowstones precipitated above alluvial sediments (Fig. 5b). Later, groundwater eroded the underlying fluvial sediments leaving the flowstone hanging on the wall. This situation results in the unstable gravitational position of these flowstones, favouring their breakdown and collapse (Fig. 4C). Furthermore, speleothems show erosive scars frequently related to the fluvial incision occurred after their precipitation.

All this information about the alluvial sediments and speleothems evidences that these deposits filled the vadose canyons and phreatic/epiphreatic conduits in the past. Therefore, at least, a phase of cave filling and another one of cave erosion occurred during cave evolution.

Slackwater deposits comprising up to 4 m-thick deposits of carbonate silts and clays are often preserved along the walls or at the bottom of phreatic/epiphreatic conduits (Fig. 2). Quartz grains are also frequent in these sediments. These deposits are either massive or show a fine-lamination marked by millimeter-scale fining-upward sequences. In few cases, these sediments cover fluvial and breakdown deposits. In the Torca La Texa cave, Ballesteros et al. (2017) interpreted two of these deposits as rhythmites formed during floods caused by glacial melting in the MIS 5c-b; thus these sediments come from glacial erosion of the limestone.

Lastly, fluvial deposits, slackwater sediments, or flowstones and dripstones usually cover debris deposits by cave breakdown (Fig. 2). This process is very common in the studied cavities, especially in the breakdown-modified passages, where accumulations of up to 7 m of fallen debris were recognized. Nowadays, breakdown processes continue to actively modify the cave morphologies and their deposits, especially perched speleothems mentioned above.

4.3 Cave geochronology

Table 2 displays 28 new $^{234}\text{U}/^{230}\text{Th}$ dates. The majority of speleothem samples contain siliciclastic material (clays), increasing detrital ^{230}Th . However, terrigenous contamination by detrital Th is negligible as the $^{230}\text{Th}/^{232}\text{Th}$ ratio in almost all samples is greater than one or two.

Fig. 7 displays the geomorphological setting of the dated speleothems and alluvial deposits in the pilot caves, providing the spatial and temporal relationships between the speleothems, fluvial, slackwater and breakdown deposits. Table 3 shows a single burial $^{26}\text{Al}/^{10}\text{Be}$ age for a sample collected from a fluvial deposit located in the Torca Teyera cave. This date provides a reference age of 2.1 ± 0.5 Ma for the alluvial deposition at the 700-800 m cave level. Despite the fact, we only have one burial age, the obtained age allowed us to estimate an erosion rate of 0.01 mm a^{-1} for the study area since the Pliocene. This value only allows us to assess the order of magnitude of regional erosion.

4.4 Karst massif and field relationship between caves and surficial landforms

The caves are located on a karstic plateau dipping $6\text{-}10^\circ$ to the north, dominated by glacial valleys, glaciokarst depressions and dolines. This plateau shows glacial till mainly between 900-1300 m asl, (Fig. 9) containing clasts of limestone, sandstone, igneous rocks, bauxites and nodules of siderite (altered to limonite by weathering). These non-carbonate clasts are similar to the allochthonous fluvial deposits found in the pilot caves (section 4.2). As shown by the glacier reconstructions for the maximum local extent (e.g. Rodríguez-Rodríguez et al., 2014; Ruiz-Fernández et al., 2016b), the karst plateau containing most of the pilot caves was covered by glaciers, except for the Pozu Lluçia cave located in a smaller hillside without glacial evidence (Fig. 9).

Fluvial, slope and nival processes also modelled the narrow fluvial canyons surrounding the karst plateau (Fig. 9). The largest karst springs (up to $\sim 10 \text{ m}^3\cdot\text{s}^{-1}$ discharge) are located in the consequent Cares River, while karst springs with 0.01-0.2

$\text{m}^3 \cdot \text{s}^{-1}$ discharge correspond to the source of the subsequent Casaño, La Beyera, Pomperi and Hunhumia rivers. In all these cases, the springs are perched from 3 to 10 m above the river channels; nevertheless, the springs include minor discharge conduits located at the same altitude of the river. This suggests that conduit development is keeping pace with valley incision.

Fig. 9 shows the location of the known caves in relation to surface geomorphology. Many cave entrances are located in glacial valleys or cirques, or in the Cares river canyon, where surface erosion has truncated existing phreatic/epiphreatic conduits and vadose cave systems, leaving decapitated shafts (Klimchouk et al. 2006) (Fig. 10). This suggests that most surface landforms are generally younger than the truncated karst landforms. Locally, glacial valleys include karst springs that were mostly blocked in the past by glaciers and till (Fig. 10c), at least during the local maximum extension (Ballesteros et al., 2017).

5. Discussion

5.1 Generations of speleothems

The ^{34}U -Th speleothem dates and the $^{26}\text{Al}/^{10}\text{Be}$ burial age (including previous 6 ages obtained by Ballesteros et al., 2015d, 2017), and their relationship with fluvial and breakdown deposits help constrain the regional evolutionary model of cave and landscape development.

5.1.1 First generation of speleothems (>260 ka)

The oldest recognized generation of speleothems comprise seven flowstones precipitated along cave walls or over fluvial, slackwater and breakdown deposits, including large fallen blocks. These speleothems precipitated at 259 ± 59 , 287 ± 36 and 300 ± 46 ka (samples LL-20, FR-16 and FR-13) coevally with end of MIS 8 transition to MIS 7, and another five were deposited before 350 ka, whose $^{230}\text{Th}/^{234}\text{U}$ ratios are larger than one (samples TEY-03, TEY-04, TEX-04, FR-03, FR-10 and FR-17) (Table

2). Therefore, fluvial and slackwater deposits were covered by the first generation of speleothems that took place before the end of MIS 7 (Fig. 8). Locally, the samples FR-03, FR-10 and FR-13 precipitated mainly above fallen boulders, thus they post-dated collapse events that occurred prior to 254/350 ka.

5.1.2 Second generation of speleothems (220-145 ka)

The second generation of speleothems involves seven flowstones related to cave deposits. The samples TEX-01 and TEX-03 are located on top of fluvial deposits, while the sample TEY-02 belongs to a flowstone interlayered into a fluvial terrace deposit, and the sample FR-15 is a flowstone ledge interbedded within a fluvial deposit (Fig. 7s). The sample FR-14 covered a fallen boulder post-dating the rock-fall process (Fig. 7r) while the sample FR-11 is located above a previous slackwater deposit (Fig. 7q). The ages of these samples are between 156 ± 12 ka and 205 ± 19 ka, suggesting that this second generation is associated with the fluvial sedimentation that took place during the MIS 7-6. These fluvial sediments almost filled the pilot caves (Fig. 7; section 4.2) owing to the presence of an ancient pavement of the cave higher than the current cave floor. Later, the cave water eroded most of the fluvial sediments causing the collapse of the flowstone that were precipitated above them. The remains of these flowstones are preserved as ledges in the cave walls at the present day. The samples TEY-02, TEX-01, FR-11 and FR-15 show evidence of water erosion that likely occur after 145 ka (Fig. 8).

5.1.3 Third generation of speleothems (125-45 ka)

The third generation of speleothems comprises flowstones (samples FR-09, FR-12, LL-15, LL-17, LL-21 and LL-24), and one stalagmite (sample LL-13) precipitated in vadose canyons and on top of cave deposits that display erosive scars created by cave streams. This speleothem generation also involves one pool deposit (sample TEX-02) and two flowstones interbedded in slackwater deposits (samples TEX-21 and TEX-

24B). In general, these speleothems precipitated on erosive surfaces between 126 ± 11 and 45 ± 3 ka (Table 2), and also show frequently erosive scars. This suggests the development of a general erosive period coeval to the precipitation of the third speleothem generation, from 125 to 45 ka (~MIS 5-4). In El Frailín de Camplengu, the stalagmite FR-12 (124 ± 20 ka) grew above the eroded stalagmite FR-14 (219 ± 20 ka) of the second generation (Fig. 7q). Locally cave sedimentation occurred marked by the growth of a pool deposit at 65 ± 6 ka (sample TEX-02) associated with a small paleolake (Fig. 7g) (Ballesteros et al., 2015a), and by the deposition of slackwater deposits at 109 ± 7 (TEX-21) ka and 95 ± 6 ka (TEX-24B), (Fig. 7j, k) (Ballesteros et al., 2017).

5.1.4 Fourth generation of speleothems (<25 ka)

The fourth generation of speleothems comprises the four flowstone precipitated on cave deposits, two stalagmites located on top of previous slackwater deposits and flowstones, and one small stalactite formed on a cave wall. The ages of these speleothems range from 22 ± 2 to 1.33 ± 0.09 ka and define the timing of the fourth generation since 25 ka (~MIS 2-1). The flowstone LL-22 precipitated over the flowstone LL-21 of the third generation evidencing the presence of a sedimentary hiatus from 22 ± 2 to 63 ± 3 ka (~MIS 3) (Fig. 7ab).

5.2 Regional evolution model

We propose a speleogenetic model of Picos de Europa based on geomorphological and geochronological evidence previously described, and includes six phases (Fig. 11). Phases 1 and 2 correspond to the origin and main development of the cave conduits, while phases 3-6 represent the evolution of the caves since the Upper Middle Pleistocene. The presence of cave levels up to 2400 m altitude points out that karstification in Picos de Europa started before phase 1 because the studied cave levels are located up to 1300 m a.s.l. (Ballesteros et al., 2015b).

5.2.1 Phase 1: main cave levels development during Pliocene

The development of the main cave levels between 700 and 1300 m altitude most probably took place during phase 1 (Fig. 11). The phreatic flow was orientated to the SE, supplying the Cares River, except for Torca Teyera that drained to the N. During this first phase, Picos de Europa would have been an uplifting mountain area already divided in the current three massifs by the developing gorges of the consequent Cares, Sella and Deva rivers (Fig. 12a). The main surface of the landscape probably dipped to the N and the Permian-Mesozoic rocks covered (partially to completely) the karstified limestone (Smart, 1984, 1986; Fernández-Gibert et al., 2000).

The cosmogenic age (2.1 ± 0.5 Ma) obtained from fluvial deposits from the 700-800 m cave level is consistent with a Pliocene age suggested by Smart (1986) and Fernández-Gibert et al. (2000). The vertical elevation range between dated fluvial sediment (930 m a.s.l.) and the elevation of the water table currently located below the Torca Teyera cave (400 m a.s.l.) is 530 m; therefore, the rate of base-level lowering over the last 1.6-2.6 Ma can be estimated as $0.15\text{-}0.25 \text{ mm}\cdot\text{a}^{-1}$. This value is one order of magnitude higher than the inferred erosive rate (0.01 mm a^{-1}) calculated for the same period using ^{26}Al and ^{10}Be radioisotopes (section 4.3), thus the age of the cave would be older than 2.1 Ma.

The highest cave level of Picos de Europa is located at 2400 m in the Central Massif, with its current water table located at 315 m a.s.l. (Ballesteros et al., 2015b, 2015d). Assuming a constant rate of base-level lowering of $0.15\text{-}0.25 \text{ mm}\cdot\text{a}^{-1}$ for the drop of the water table (2085 m), we infer in 8.8-13.5 Ma the hypothetic age for the oldest cave level of Picos de Europa. This suggests that initial karstification occurred during the Miocene.

Following previous studies (Strasser et al., 2009; Wagner et al., 2010), we consider that the rate of tectonic uplift is similar to the rate of base-level lowering, resulting in a

rate of around $0.15\text{--}0.25\text{ mm}\cdot\text{a}^{-1}$ since the Pliocene. This value is consistent with the rates deduced by geomorphological and thermochronological studies in the Cantabrian Mountains (Table 4). The obtained rate is similar to the rates proposed for the Pliocene-Quaternary and is one order of magnitude larger than the rates proposed for the Neogene-Paleogene in the Cantabrian Mountains. A rejuvenation of the relief during the Pliocene can explain these differences, as it was suggested by apatite fission track dating in the Pyrenees (Babault et al., 2005; Jolivet et al., 2007).

5.2.2 Phase 2: main development of vadose conduits during the Calabrian-Middle Pleistocene

Valley incision and the erosion of the Alpine sedimentary cover after the Pliocene triggered the descent of the regional water tables and the subsequent extension of the vadose zone. Fluvial incision and lateral migration of cave streams modified the geometry of phreatic/epiphreatic conduits (Fig. 11b, d) and developed vadose canyons and shafts that intercepted previous conduits. Paragenetic features (pendants, corrosion notches) likely occurred during this phase. New vadose canyons also formed as well as the formation of the second generation of speleothems before and during the MIS 8 (Fig. 11d). Major breakdown and collapse events occurred during this phase because flowstones with more than $\sim 220\text{ ka}$ cover the largest fallen boulders (samples FR-03, FR-13 and FR-14; section 4.3). All these processes generated the current general configuration of caves geometry, producing later variations in their infill. The change from phreatic to vadose conditions allowed the precipitation of first generation of speleothems before 260 ka .

The landscape of the second phase would be similar to the first one, although the extent of the Alpine sedimentary cover was smaller and the river canyons were deeper than in Phase 1 (Fig. 12b). This situation would allow the development of dolines and the border polje of Vega de Comeya. Glaciers occupied at least the highest areas before $394\text{--}276\text{ ka}$ (Villa et al., 2013). In the NW of Picos de Europa, the development

of the subsequent Casaño River flowing to the N began during this phase, developing its canyon and capturing the groundwater of the surroundings of Torca La Texa and Pozu Lluçia (Fig. 12b). Therefore, the groundwater of these caves changed their drainage directions from the SE in Phase 1 to the N in Phase 2. Nowadays, the groundwater continues to flow to the N and emerges in the spring of the Casaño River (Ballesteros et al., 2015a, 2015d).

5.2.3 Phase 3: cave sedimentary infill at 220-145 ka (~MIS 7-6)

The third phase of the speleogenetic model is based on the reconstruction of caves fluvial infill (section 4.2) and the second generation of speleothems, whose age is considered as a reference timing for the cave filling (section 4.3). These sediments filled the cavities almost completely, thus the ancient pavement of the caves was located higher than nowadays. The infill favoured the development of pendants under paragenetic conditions (Fig. 11). Considering U/Th ages, Phase 3 took place during MIS 7-6.

The landscape reached the current configuration at a regional scale during Phase 3 (Fig. 12c). The Alpine sedimentary cover was almost completely eroded, at least in the surroundings of the pilot caves. Fluvial sediments contain allochthonous clasts derived from the erosion of Stephanian (~Kasimovian) sandstone (with siderite nodules) and igneous rocks that cropped out to the S of the study area. The igneous rocks correspond to the andesite and basaltic dykes described by Ballesteros et al. (2011a) and located toward the SW of the pilot caves. Considering all this information, the landscape of phase 3 presented a developing karst plateau with outcrops of Stephanian sandstone and shale (Fig. 12c).

5.2.4 Phase 4: cave erosion at 125-45 ka (~MIS 5-3)

The erosion of the sedimentary sequences formed during phase 3 defines the fourth phase of the speleogenetic model. During this phase, the small speleothems of the

third generation precipitated on top of the erosive surfaces developed along the walls of vadose conduits or on cave deposits (section 4.3). This generation of speleothem deposition (125-45 ka) took place between MIS 5 and 3. Simultaneously, fluvial erosion partially eroded fluvial sediments and speleothems of the first and second generations, leaving erosional remnants as terraces above the cave floor (Fig. 11). Breakdown processes affected these speleothems and, sometimes, triggered their collapse (for instance, samples FR-09, FR-17 and FR-18). This situation provoked the formation of “false floors” (hanging ancient speleothem pavements), very common in caves of Picos de Europa (Sefton, 1984; Smart, 1984) and the Cantabrian Mountains (Gázquez et al., 2014).

In the Cantabrian Mountains, the presence of fluvial terraces older than 47-48 ka and other terraces with inferred ages of Upper Pleistocene suggest a general fluvial incision between 120 and 50 ka (González Díez et al., 1996; Ruiz-Fernández and Poblete Piedrabuena, 2011) in accordance with the general erosion of the cave infill.

Furthermore, during this phase, the karst landscape involved still minor outcrops of sandstone that were eroding (Fig. 12d), as evidenced by the presence of sandstone clasts in the till (section 4.4) and minerals in the glacial cave rhythmites (Ballesteros et al., 2017). These sediments also indicated that glaciers should have occupied the areas located at least at 1300 m of altitude during the ~MIS 5d-c. The presence of glaciers in phase 4 agrees with the development of a glacial paleolake with a minimum age of 46 ka in the border polje of Vega de Comeya (Jiménez-Sánchez et al., 2013) and with the maximum glacial local extension dated at 114 ± 8 ka in the neighboring Central Cantabrian Mountains (Rodríguez-Rodríguez et al., 2016). The glaciers intercepted previous vadose and phreatic/epiphreatic conduits recognized in the study area (section 4.4), blocking the karst springs located above 800 m a.s.l. (Ballesteros et al., 2017). The geomorphological map of the study area indicates that the surroundings of the Pozu Lluvia cave was ice-free, at least, during the Upper Pleistocene (Fig. 12d).

This situation suggests that liquid water would have been more available: This would favour a speleothem growth greater than other pilot caves located in areas covered by glaciers.

5.2.5 Phase 5: speleothem apparent pause at 45-25 ka (~MIS 3-2)

Phase 5 represents a general apparent pause in the speleothem (Fig. 11). The combination of five arguments supports this hypothesis: (1) no speleothems deposited between 45 and 25 ka have been found so far in the pilot caves (Fig. 8); (2) the speleothem growth of Pozu Lluvia cave displays a hiatus between the precipitation of flowstones LL-22 (22 ± 2 ka) and LL-21 (63 ± 3 ka), (3) the content of carbonates of the Enol Lake (Fig. 9) decreased between 38 and 17 ka (Moreno et al., 2010), (4) cryogenic processes took place in the Belbin depression from 37 to 29 ka (Fig. 9) (Nieuwendam et al., 2015); and (5) the development of dry and cold conditions during the MIS 3-2 in the Cantabrian Mountains (Álvarez-Lao et al., 2015; Uzquiano et al., 2016).

The landscape present during this phase corresponds to a karst covered by glaciers, whose extension varied temporally, reaching the 1000 m of altitude, at least, at ca 40-45 ka (Fig. 12e) (Jiménez-Sánchez and Farias, 2002; Moreno et al., 2010; Nieuwendam et al., 2015). The variation of the ice extension was coeval with a general glacial retreat up to beginning of the Last Glacial Maximum (LGM), at 23-25 ka in the Cantabrian Mountains (Rodríguez-Rodríguez et al., 2014; Serrano et al., 2016). Frost weathering and solifluction processes modelled the ice-free areas (Nieuwendam et al., 2015). Locally, lacustrine environments occupied glacial and karst depressions, as with the Enol Lake (since 38 ka) and the paleolake of border polje of Vega de Comeya (Fig. 12e) (Moreno et al., 2010). This paleolake was completely filled at 3-4 ka (Farias et al., 1996).

The dry and cold conditions, combined with glacial and periglacial activities, decreased the recharge of the karst aquifer. In carbonates, environments with less -5°C average annual temperature can limit strongly the groundwater flow in the endokarst (Ford, 1993). The water scarcity agrees with the flowstone precipitation above the thalweg deposits; however, the high detrital content of these speleothems hampers their dating using the uranium-series decay method.

5.2.6 Phase 6: speleothem reactivation since 25 ka (~MIS 3-2)

The precipitation of the fourth generation of speleothems defines the last phase of the speleogenetic model (Fig. 11). This phase represents a reactivation of the speleothem precipitation respect to the hypothetical phase 5. Fluvial sedimentation and speleothem formation increased in the pilot caves, precipitating mainly dripstone and flowstone on top of previous deposits.

The glacial advances related to LGM took place during phase 6, descending up to 1000 m in the Vega del Brial before 11 ka (Fig. 12f) (Ruiz-Fernández et al., 2013), however, they did not supply water to the Enol Lake since 26 ka (Moreno et al., 2010). Subsequently, the glaciers retreated up to the cirques, disappearing almost completely in the Holocene (Fig. 12g). Nowadays, the incision of cave streams continues and karst springs are perched above the surface rivers (section 4.4). Consequently, the karstification continues to develop down to the base level marked by river position, evidencing that the caves and rivers are at disequilibrium and the fluvial incision still continues. This situation suggests that Picos de Europa is uplifting at least up to the present.

6. Conclusions

The geomorphologic regional history of the Picos de Europa based on the geomorphology and speleogenesis of four alpine caves has been reconstructed based on 34 $^{234}\text{U}/^{230}\text{Th}$ speleothem ages, the first $^{26}\text{Al}/^{10}\text{Be}$ burial dating performed in Picos de

Europa, and the relationship between caves and surface processes of the glaciated karst massif. The 12 km of conduits in four pilot caves comprise 47 % of vadose canyons and shafts, 45 % of phreatic/epiphreatic conduits organised in six cave levels from 600 to 1300 m a.s.l., and 7 % of breakdown-modified passages.

Six phases constitute the speleogenetic model since the Pliocene although the cave evolution might have begun in the Miocene. We inferred the uplift rate of Picos de Europa at $0.15\text{--}0.25\text{ mm}\cdot\text{a}^{-1}$ since $2.1 \pm 0.5\text{ Ma}$.

- Phase 1 (Pliocene): development of a karst partially or totally covered by an Alpine sedimentary cover, showing the incipient forming canyons of the consequent rivers of the region. Coevally, the main development of cave levels of 800-1300 m altitude was formed by a SE-directed flow in the Western Massif of Picos de Europa. Phreatic flow was toward the Cares River which incision favoured the descent of the water tables.
- Phase 2 (Calabrian to Middle Pleistocene): erosion of the Permian-Mesozoic cover and capture of the northern Western Massif by the Casaño River. Vadose canyons and shafts were developed, affected by locally important breakdown processes.
- Phase 3 (220-145 ka, ~MIS 7-6): cave infill by speleothems and fluvial sediments derived from the erosion of Stephanian sandstone and shale that crops out locally in the highest areas of Picos de Europa.
- Phase 4 (125-45 ka, ~MIS 5-3): erosion of the previous cave infill by fluvial incision.
- Phase 5 (45-25 ka, ~MIS 3-2): apparent pause in the speleothem deposition under a dry and cold environment dominated by glacial retreat and cryogenic processes.
- Phase 6 (since 25 ka; ~MIS 2-1): reactivation of the speleothem precipitation and speleothem precipitation by a general increase of temperature and

precipitation. This phase coincides with a slight warming at 26 ka, glacial advances during the LGM, and their retreat to the glacial cirque up to their demise in the Holocene.

The main factors of the evolution of Picos de Europa and its caves would be glacial activity at least since the MIS 7, the fluvial incision of consequent rivers, fluvial captures of subsequent rivers, and the erosion of the Stephanian detrital rocks in the higher areas of Picos de Europa.

The proposed speleogenetic model evidences the usefulness of the alpine cave studies for reconstructing the geomorphologic evolution of a region for Quaternary times, integrating information about the relief uplift, river incision, water table evolution, and glaciations.

Acknowledgements

This work is a contribution of the GeoQUO and GeoCantabrian Research Groups (University of Oviedo) funded through the GEOCAVE project (MAGRAMA-580/12-OAPN). We are grateful to P. Häuselmann (ISSKA) for help to calculate the cosmogenic date, to GE Polifemo, GES M Celtas, AD GEMA and G. Sendra for their collaboration and their help during the fieldwork, and to the Picos de Europa National Park for the provided facilities. The manuscript was improved by useful comments done by J. De Waele and another anonymous reviewer. Cave data of Fig. 1 are courtesy of GE Polifemo, OUCC, GE Diañu Burlón, AD Cuasacas, S Wroclaw, SIS-CE Terrassa, Expeditions to Castil, GE Gorfolí, GE Matallana, GEMA, CDG, CADE, SEB Escar, SIE Áliga, GEG, WCC, GET, SSS, IEV, Cocktail Picos, YUCPC, AD Kami, Llabrión-Project, ERE, SCOF, GES CMT, STD-BAT, CES Alfa and AS Charentaise, GERSOP, GS Matese, GSD, HPS, L'Esperteyu CEC, LUSS, SAR d'Ixelles, GE Llubí, ANEM, and SCS Matese. National Geographic Institute of Spain provided topographic and aerial photography data. We dedicate this work to the memory of J. Gambino,

brilliant speleologist, good geologist and great friend, who contributed greatly to explore and research deep caves in Picos de Europa.

References

- Álvarez-Lao, D.J., Ruiz-Zapata, M., Gil-García, M., Ballesteros, D., Jiménez-Sánchez, M., 2015. Palaeoenvironmental research at Rexidora Cave: new evidence of cold and dry conditions in NW Iberia during MIS 3. *Quat. Int.* 379, 35–46.
- Alvarez-Marrón, J., Hetzel, R., Niedermann, S., Menéndez, R., Marquínez, J., 2008. Origin, structure and exposure history of a wave-cut platform more than 1 Ma in age at the coast of northern Spain: A multiple cosmogenic nuclide approach. *Geomorphology* 93, 316–334.
- Aranburu, A., Arriolabengoa, M., Iriarte, E., Giralt, S., Yusta, I., Martínez-Pillado, V., del Val, M., Moreno, J., Jiménez-Sánchez, M., 2014. Karst landscape evolution in the littoral area of the Bay of Biscay (north Iberian Peninsula). *Quat. Int.* 367, 217–230.
- Arnold, M., Merchel, S., Bourlès, D.L., Braucher, R., Benedetti, L., Finkel, R.C., Aumaître, G., Gott dang, A., Klein, M., 2010. The French accelerator mass spectrometry facility ASTER: Improved performance and developments. *Nucl. Instruments Methods Phys. Res. Sect. B Beam Interact. with Mater. Atoms* 268, 1954–1959.
- Audra, P., Quinif, Y., Rochette, P., 2002. The genesis of Tennengerbirge karst and caves (Salzburg, Austria). *J. Cave Karst Stud.* 64, 153–164.
- Audra, P., Bini, A., Gabrovšek, F., Häuselmann, P., Hobléa, F., Jeannin, P.-Y., Kunaver, J., Monbaron, M., Šušteršič, F., Tognini, P., Trimmel, H., Wildberger, A., 2006. Cave genesis in the Alps between the Miocene and today: a review. *Zeitschrift für Geomorphol.* 50, 153–176.

- Ayala Carcedo, F., Rodríguez Ortiz, J., Del Val Melus, J., Durán Valsero, J., Prieto Alcolea, C., Rubio Amo, J., 1986. Memoria del mapa del karst de España. Instituto Geológico y Minero de España, Madrid, Spain.
- Babault, J., Van Den Driessche, J., Bonnet, S., Castelltort, S., Crave, A., 2005. Origin of the highly elevated Pyrenean peneplain. *Tectonics* 24, 1–19.
- Bahamonde, J.R., Merino-Tomé, O., Heredia, N., 2007. A Pennsylvanian microbial boundstone-dominated carbonate shelf in a distal foreland margin (Picos de Europa Province, NW Spain). *Sediment. Geol.* 198, 167–193.
- Ballesteros, D., Cuesta, A., Rubio-Ordóñez, A., 2011a. Actividad ígnea filoniana en los Picos de Europa (N de España): basaltos, lamprófidos y andesitas. *Geogaceta* 50, 55–58.
- Ballesteros, D., Jiménez-Sánchez, M., García-Sansegundo, J., Giralt, S., 2011b. Geological methods applied to speleogenetical research in vertical caves: the example of Torca Teyera shaft (Picos de Europa, Northern Spain). *Carbonates and Evaporites* 26, 29–40.
- Ballesteros, D., Jiménez-Sánchez, M., Giralt, S., García-Sansegundo, J., Meléndez-Asensio, M., 2015a. A multi-method approach for speleogenetic research on alpine karst caves. Torca La Texa shaft, Picos de Europa (Spain). *Geomorphology* 247, 35–54.
- Ballesteros, D., Malard, A., Jeannin, P.-Y., Jiménez-Sánchez, M., García-Sansegundo, J., Meléndez-Asensio, M., Sendra, G., 2015b. Influence of the rivers on speleogenesis combining KARSYS approach and cave levels. Picos de Europa, Spain, in: Andreo, B., Carrasco, F., Durán, J.J., Jiménez, P., LaMoreaux, J.W. (Eds.), *Hydrogeological and Environmental Investigations in Karst Systems*, Environmental Earth Sciences. Springer, Berlin, pp. 599–607.

- Ballesteros, D., Malard, A., Jeannin, P.-Y., Jiménez-Sánchez, M., García-Sansegundo, J., Meléndez-Asensio, M., Sendra, G., 2015d. KARSYS hydrogeological 3D modeling of alpine karst aquifers developed in geologically complex areas. Picos de Europa National Park. *Environ. Earth Sci.* 74, 7699–7714.
- Ballesteros, D., Jiménez-Sánchez, M., Giralt, S., DeFelipe, I., García-Sansegundo, J., 2017. Glacial origin for cave rhythmite during MIS 5d-c in a glaciokarst landscape, Picos de Europa (Spain). *Geomorphology* 286, 68–77.
- Berenguer-Sempere, F., Gómez-Lende, M., Serrano, E., Sanjosé-Blasco, J.J. de, 2014. Orthothermographies and 3D modeling as potential tools in ice caves studies: the Peña Castil Ice Cave. *Int. J. Speleol.* 43, 35–43.
- Bischoff, J.L., Julià, R., Mora, R., 1988. Uranium-series dating of the Mousterian occupation at Abric Romaní, Spain. *Nature* 332, 68–70.
- Bischoff, J.L., Fitzpatrick, J.A., 1991. U-series dating of impure carbonates: An isochron technique using total-sample dissolution. *Geochim. Cosmochim. Acta* 55, 543–554.
- Calvet, M., Gunnell, Y., Braucher, R., Hez, G., Bourlès, D., Guillou, V., Delmas, M., 2015. Cave levels as a proxy for measuring post-orogenic uplift: Evidence from cosmogenic dating of alluvium-filled caves in the French Pyrenees. *Geomorphology* 246, 617–633.
- Chmeleff, J., von Blanckenburg, F., Kossert, K., Jakob, D., 2010. Determination of the ^{10}Be half-life by multicollector ICP-MS and liquid scintillation counting. *Nucl. Instruments Methods Phys. Res. Sect. B Beam Interact. with Mater. Atoms* 268, 192–199.
- Columbu, A., De Waele, J., Forti, P., Montagna, P., Picotti, V., Pons-Branchu, E., Hellstrom, J., Bajo, P., Drysdale, R. N., 2015. Gypsum caves as indicators of

- climate-driven river incision and aggradation in a rapidly uplifting region. *Geology* 43(6), 539-542
- De Waele, J., Pasini, G., 2013. Intra-messinian gypsum palaeokarst in the Northern Apennines and its palaeogeographic implications. *Terra Nov.* 25, 199–205.
- Eme, D., Malard, F., Colson-Proch, C., Jean, P., Calvignac, S., Konecny-Dupré, L., Hervant, F., Douady, C.J., 2014. Integrating phylogeography, physiology and habitat modelling to explore species range determinants. *J. Biogeogr.* 41, 687–699.
- Erra, J., Genuite, P., Renous, N., Vidal, B., 1999. La Torca del Cerro (-1589) et le secteur du Trave. *Spelunca* 74, 26–50.
- Fairchild, I., Spötl, C., Frisia, S., Borsato, A., Susini, J., Wynn, P.M., Cauzid, J., EMIF, 2010. Petrology and geochemistry of annually laminated stalagmites from an Alpine cave (Obir, Austria): seasonal cave physiology, in: Pedley, H., Rogerson, M. (Eds.), *Special Publication 336: Tufas and Speleothems: Unravelling the Microbial and Physical Controls*. Geological Society of London, London, pp. 295–321.
- Farias, P., Jiménez, M., Marquínez, J., 1996. Nuevos datos sobre la estratigrafía del relleno cuaternario de la depresión de Comeya (Picos de Europa, Asturias). *Geogaceta* 20, 116–119.
- Farrant, A.R., P.L. Smart, 2011. Role of sediments in speleogenesis; sedimentation and paragenesis. *Geomorphology* 134, 79–93.
- Fernández-Gibert, E., Calaforra, J.M., Rossi, C., 2000. Speleogenesis in the Picos de Europa Massif, Northern Spain, in: Klimchouk, A., Ford, D., Palmer, A., Dreybrodt, W. (Eds.), *Speleogenesis: Evolution of Karst Aquifers*. National Speleological Society, Huntsville, pp. 352–357.

- Fillon, C., Pedreira, D., Van Der Beek, P.A., Huismans, R.S., Barbero, L., Pulgar, J.A., 2016. Alpine exhumation of the central Cantabrian Mountains, Northwest Spain. *Tectonics* 35, 339–356.
- Ford, D.C., 1987. Effects of glaciations and permafrost upon the development of karst in Canada. *Earth Surf. Process. Landforms* 12, 507–521.
- Ford, D.C., 1993. Karst in cold environments, in: French, H.M., Slaymaker, O. (Eds.), *Canada's Cold Environments*. McGill-Queen's University Press, Quebec, pp. 199–222.
- Gallastegui, J., Pulgar, J.A., Gallart, J., 2016. Alpine tectonic wedging and crustal delamination in the Cantabrian Mountains (NW Spain). *Solid Earth* 7, 1043–1057.
- Gázquez, F., Calaforra, J.M., Forti, P., Stoll, H., Ghaleb, B., Delgado-Huertas, A., 2014. Paleoflood events recorded by speleothems in caves. *Earth Surf. Process. Landforms* 39, 1345–1353.
- Goldscheider, N., Neukum, C., 2010. Fold and fault control on the drainage pattern of a double-karst-aquifer system, Winterstaude, Austrian Alps. *Acta Carsologica* 39, 173–186.
- González-Trueba, J., Martín Moreno, R., Martínez de Pisón, E., Serrano, E., 2008. 'Little Ice Age' glaciation and current glaciers in the Iberian Peninsula. *The Holocene* 18, 551–568.
- González Díez, A., Salas, L., Díaz de Terán, J., Cendrero, A., 1996. Late Quaternary climate changes and mass movement frequency and magnitude in the Cantabrian region, Spain. *Geomorphology* 15, 291–309.
- Granger, D.E., Fabel, D., Palmer, A.N., 2001. Pliocene-Pleistocene incision of the Green River, Kentucky, determined from radioactive decay of cosmogenic ^{26}Al and ^{10}Be in Mammoth Cave sediments. *Geol. Soc. Am. Bull.* 113, 825–836.

- Grobe, R.W., Alvarez-Marrón, J., Glasmacher, U.A., Stuart, F.M., 2014. Mesozoic exhumation history and palaeolandscape of the Iberian Massif in eastern Galicia from apatite fission-track and (U+Th)/He data. *Int. J. Earth Sci.* 103, 539–561.
- Hallstadius, L., 1984. A method for the electrodeposition of actinides. *Nucl. Instruments Methods Phys. Res.* 223, 266–267.
- Häuselmann, P., 2011. UIS Mapping Grades. *Int. J. Speleol.* 40, IV–VI.
- Häuselmann, P., 2013. Large epigenic caves in high-relief areas, in: Shroder, J., Frumkin, A. (Eds.), *Treatise on Geomorphology*, Vol 6, Karst Geomorphology. Academic Press, San Diego, USA, pp. 207–219.
- Häuselmann, P., Granger, D.E., Jeannin, P.-Y., Lauritzen, S.-E., 2007. Abrupt glacial valley incision at 0.8 Ma dated from cave deposits in Switzerland. *Geology* 35, 143–146.
- Hobléa, F., Häuselmann, P., Kubik, P., 2011. Cosmogenic nuclide dating of cave deposits of Mount Granier (Hauts de Chartreuse Nature Reserve, France): morphogenic and palaeogeographical implications. *Géomorphologie Reli. Process. Environ.* 4, 395–406.
- Ivanovich, M., Harmon, R.S., 1992. Uranium-series disequilibrium: applications to Earth, Marine, and Environmental Sciences. Oxford, Clarendon Press, 910 pp.
- Jiménez-Sánchez, M., Farias, P., 2002. New radiometric and geomorphologic evidences of a last glacial maximum older than 18 ka in SW European mountains: the example of Redes Natural Park (Cantabrian Mountains, NW Spain). *Geodin. Acta* 15, 93–101.
- Jiménez-Sánchez, M., Bishoff, J., Stoll, H., Aranburu, A., 2006. A geochronological approach for cave evolution in the Cantabrian Coast (Pindal Cave, NE Spain). *Zeitschrift für Geomorphol. Suppl.* Vol. 147, 129–141.

- Jiménez-Sánchez, M., Rodríguez-Rodríguez, L., García-Ruiz, J.M., Domínguez-Cuesta, M.J., Farias, P., Valero-Garcés, B., Moreno, A., Rico, M., Valcárcel, M., 2013. A review of glacial geomorphology and chronology in northern Spain: Timing and regional variability during the last glacial cycle. *Geomorphology* 196, 50–64.
- Johnston, V.E., Borsato, A., Spötl, C., Frisia, S., Miorandi, R., 2013. Stable isotopes in caves over altitudinal gradients: fractionation behaviour and inferences for speleothem sensitivity to climate change. *Clim. Past* 9, 99–118.
- Jolivet, M., Labaume, P., Monié, P., Brunel, M., Arnaud, N., Campani, M., 2007. Thermochronology constraints for the propagation sequence of the south Pyrenean basement thrust system (France-Spain). *Tectonics* 26, 1–17.
- Klimchouk, A., Bayari, S., Nazik, L., Törk, K., 2006. Glacial destruction of cave systems in high mountains, with a special reference to the Aladaglar massif, Central Taurus, Turkey. *Acta Carsologica* 35, 111–121.
- Larsen, W., Mangerud, J., 1989. Marine Caves: on-off signals for glaciations. *Quat. Int.* 3/4, 13–19.
- Lauritzen, S., Skoglund, R.Ø., 2013. Glacier ice-contact speleogenesis in marble stripe karst, in: Shroder, J., Frumkin, A. (Eds.), *Treatise on Geomorphology*, Vol 6, Karst Geomorphology. Academic Press, San Diego, pp. 363–396.
- Luetscher, M., Boch, R., Sodemann, H., Spötl, C., Cheng, H., Edwards, R.L., Frisia, S., Hof, F., Müller, W., 2015. North Atlantic storm track changes during the Last Glacial Maximum recorded by Alpine speleothems. *Nat. Commun.* 6, 6344.
- Maire, R., 1990. La haute montagne calcaire. *Karstologia Mémoires* 3, 731.
- Martín-González, F., Barbero, L., Capote, R., Heredia, N., Gallastegui, G., 2011. Interaction of two successive Alpine deformation fronts: constraints from low-

- temperature thermochronology and structural mapping (NW Iberian Peninsula). *Int. J. Earth Sci.* 101, 1331–1342.
- Merino-Tomé, O., Bahamonde, J.R., Colmenero, J.R., Heredia, N., Villa, E., Farias, P., 2009. Emplacement of the Cuera and Picos de Europa imbricate system at the core of the Iberian-Armorican arc (Cantabrian zone, north Spain): New precisions concerning the timing of arc closure. *Geol. Soc. Am. Bull.* 121, 729–751.
- Miorandi, R., Borsato, A., Frisia, S., Fairchild, I.J., Richter, D.K., 2010. Epikarst hydrology and implications for stalagmite capture of climate changes at Grotta di Ernesto (NE Italy): results from long-term monitoring. *Hydrol. Process.* 24, 3101–3114.
- Moreno, A., López-Merino, L., Leira, M., Marco-Barba, J., González-Sampériz, P., Valero-Garcés, B., López-Sáez, J., Santos, L., Mata, P., Ito, E., 2011. Revealing the last 13,500 years of environmental history from the multiproxy record of a mountain lake (Lago Enol, northern Iberian Peninsula). *J. Paleolimnol.* 46, 327–349.
- Moreno, A., Valero-Garcés, B.L., Jiménez-Sánchez, M., Domínguez-Cuesta, M.J., Mata, M., Navas, A., González-Sampériz, P., Stoll, H., Farias, P., Morello, M., Corella, J., Rico, M., 2010. The last deglaciation in the Picos de Europa National Park (Cantabrian Mountains). *J. Quat. Sci.* 25, 1076–1091.
- Nieuwendam, A., Ruiz-Fernández, J., Oliva, M., Lopez, V., Cruces, A., Freitas, M.C., 2015. Postglacial landscape changes and cryogenic processes in Picos de Europa (northern Spain) reconstructed from geomorphological mapping and microstructures on quartz grains. *Permafr. Periglac. Process.* 27, 96–108.
- Palmer, A. 1987. Cave levels and their interpretation. *National Speleological Society Bulletin* 49, 50–66

- Plan, L., Filipponi, M., Behm, M., Seebacher, R., Jeutter, P., 2009. Constraints on alpine speleogenesis from cave morphology — A case study from the eastern Totes Gebirge (Northern Calcareous Alps, Austria). *Geomorphology* 106, 118–129.
- Plan, L., Grasemann, B., Spotl, C., Decker, K., Boch, R., Kramers, J., 2010. Neotectonic extrusion of the Eastern Alps: Constraints from U/Th dating of tectonically damaged speleothems. *Geology* 38, 483–486.
- Quinif, Y., Maire, R., 1998. Pleistocene Deposits in Pierre Saint-Martin Cave, French Pyrenees. *Quat. Res.* 49, 37–50.
- Rodríguez-Rodríguez, L., Jiménez-Sánchez, M., Domínguez-Cuesta, M.J., Aranburu, A., 2014. Research history on glacial geomorphology and geochronology of the Cantabrian Mountains, north Iberia (43–42°N/7–2°W). *Quat. Int.* 364, 6–21.
- Rodríguez-Rodríguez, L., Jiménez-Sánchez, M., Domínguez-Cuesta, M.J., Rinterknecht, V., Pallàs, R., Bourlès, D., 2016. Chronology of glaciations in the Cantabrian Mountains (NW Iberia) during the Last Glacial Cycle based on in situ-produced ^{10}Be . *Quat. Sci. Rev.* 138, 31–48.
- Rodríguez-Rodríguez, L., Jiménez-Sánchez, M., Domínguez-Cuesta, M.J., Rinterknecht, V., Pallàs, R., 2017. Timing of last deglaciation in the Cantabrian Mountains (Iberian Peninsula; North Atlantic Region) based on in situ-produced ^{10}Be exposure dating. *Quat. Sci. Rev.* 171, 166–181.
- Rosenbauer, R.J., 1991. UDATE1: a computer program for the calculation of Uranium-series isotopic ages. *Comput. Geosci.* 17, 45–75.
- Rossi, C., Lozano, R.P., 2016. Hydrochemical controls on aragonite versus calcite precipitation in cave dripwaters. *Geochim. Cosmochim. Acta* 192, 70–96.
- Rossi, C., Villalain, J.J., Lozano, R.P., Hellstrom, J., 2016. Paleo-watertable definition

- using cave ferromanganese stromatolites and associated cave-wall notches (Sierra de Arnero, Spain). *Geomorphology* 261, 57–75.
- Ruiz-Fernández, J., Poblete Piedrabuena, M.Á., 2011. Las terrazas fluviales del río Cares: aportaciones sedimentológicas y cronológicas (Picos de Europa, Asturias). *Estud. Geográficos* 72, 173–202.
- Ruiz-Fernández, J., Oliva, M., García, C., Geraldès, M., Fernández-Irigoyen, J., 2013. El proceso de deglaciación de los Picos de Europa a partir de las evidencias geomorfológicas y sedimentológicas, in: Baena, R., Fernández, J., Guerrero, I. (Eds.), *El Cuaternario Ibérico: Investigación en el S. XXI*. Asociación Española para el Estudio del Cuaternario, La Rinconada, pp. 209–213.
- Ruiz-Fernández, J., Oliva, M., Cruces, A., Lopes, V., Freitas, M. da C., Andrade, C., García-Hernández, C., López-Sáez, J.A., Geraldès, M., 2016a. Environmental evolution in the Picos de Europa (Cantabrian Mountains, SW Europe) since the Last Glaciation. *Quat. Sci. Rev.* 138, 87–104.
- Ruiz-Fernández, J., Oliva, M., Hrbáček, F., Vieira, G., García-Hernández, C., 2016b. Soil temperatures in an Atlantic high mountain environment: The Forcadona buried ice patch (Picos de Europa, NW Spain). *Catena* 149 (2), 637–647.
- Sanz-López, J., Cózar, P., Blanco-Ferrera, S., 2018. Discovery of a Mississippian-early Bashkirian carbonate platform coeval with condensed cephalopod limestone sedimentation in NW Spain. *Geol. J.* 1–26.
- Sefton, M., 1984. Cave explorations around Tresviso, Picos de Europa, Northern Spain. *Cave Sci.* 11, 199–237.
- Senior, K.J., 1987. Geology and Speleogenesis of the M2 Cave System, Western Massif, Picos de Europa, Northern Spain. *Cave Sci.* 14, 93–103.
- Serrano, E., González-Trueba, J.J., González-García, M., 2012. Mountain glaciation

- and paleoclimate reconstruction in the Picos de Europa (Iberian Peninsula, SW Europe). *Quat. Res.* 78, 303–314.
- Serrano, E., Gonzalez-Trueba, J.J., Pellitero, R., Gomez-Lende, M., 2016. Quaternary glacial history of the Cantabrian Mountains of northern Spain: a new synthesis, in: Hughes, P.D., Woodward, J.C. (Eds.), *Quaternary Glaciation in the Mediterranean Mountains*. Geological Society of London, London, pp. 55–85.
- Smart, P.L., 1984. The geology, geomorphology and speleogenesis in the eastern massifs, Picos de Europa, Spain. *Cave Sci.* 11, 238–245.
- Smart, P.L., 1986. Origin and development of glacio-karst closed depressions in the Picos de Europa, Spain. *Zeitschrift für Geomorphol.* 30, 423–443.
- Stone, J.O., 2000. Air pressure and cosmogenic production. *J. Geophys. Res.* 105, 23753–23759.
- Strasser, M., Strasser, A., Pelz, K., Seyfried, H., 2009. A mid Miocene to early Pleistocene multi-level cave as a gauge for tectonic uplift of the Swabian Alb (Southwest Germany). *Geomorphology* 106, 130–141.
- Symons, D., Tornos, F., Kawasaki, K., Velasco, F., Rosales, I., 2015. Genetic constraints from paleomagnetic dating for the Aliva zinc–lead deposit, Picos de Europa Unit, northern Spain. *Miner. Depos.* 50, 953–966.
- Talvitie, N.A., 1972. Electrodeposition of actinides for alpha spectrometric determination. *Anal. Chem.* 44, 280–283.
- Uzquiano, P., Ruiz-Zapata, M.B., Gil-Garcia, M.J., Fernández, S., Carrión, J.S., 2016. Late Quaternary developments of Mediterranean oaks in the Atlantic domain of the Iberian Peninsula: The case of the Cantabrian region (N Spain). *Quat. Sci. Rev.* 153, 63–77.
- Vigna, B., Banzato, C., 2015. The hydrogeology of high-mountain carbonate areas: an

- example of some Alpine systems in southern Piedmont (Italy). *Environ. Earth Sci.* 74, 267–280.
- Villa, E., Stoll, H., Farias, P., Adrados, L., Edwards, R.L., Cheng, H., 2013. Age and significance of the Quaternary cemented deposits of the Duje Valley (Picos de Europa, Northern Spain). *Quat. Res.* 79, 1–5.
- Viveen, W., Schoorl, J.M., Veldkamp, A., van Balen, R.T., 2014. Modelling the impact of regional uplift and local tectonics on fluvial terrace preservation. *Geomorphology* 210, 119–135.
- Wackerbarth, A., Langebroek, P.M., Werner, M., Lohmann, G., Riechelmann, S., Borsato, A., Mangini, A., 2012. Simulated oxygen isotopes in cave drip water and speleothem calcite in European caves. *Clim. Past* 8, 1781–1799.
- Wagner, T., Fabel, D., Fiebig, M., Häuselmann, P., Sahy, D., Xu, S., Stüwe, K., 2010. Young uplift in the non-glaciated parts of the Eastern Alps. *Earth Planet. Sci. Lett.* 295, 159–169.
- Weremeichik, J., Mylroie, J., 2014. Glacial Lake Schoharie: An Investigative Study of Glaciolacustrine Lithofacies in Caves, Helderberg Plateau, Central New York. *J. Cave Karst Stud.* 76, 127–138.
- Zhou, G., Huang, J., Tao, X., Luo, Q., Zhang, R., Liu, Z., 2015. Overview of 30 years of research on solubility trapping in Chinese karst. *Earth-Science Rev.* 146, 183–194.

Figure Captions

Fig. 1. (a) The Iberian Peninsula showing the location of Picos de Europa. (b) Karst areas of the Cantabrian Mountains (after Ayala Carcedo et al., 1986). (c) Relief and fluvial network of Picos de Europa divided into three massifs by the deep fluvial valleys.

Main karst springs and more than 410 km of caves documented by speleologists are plotted.

Fig. 2. (a) Speleological map of El Frailín de Camplengu shaft. (b) Geomorphological maps of the NW (b) and SE (c) parts of the shaft. (d) Geomorphological map of the shaft Pozu Lluçia; (e), (f) and (g) shows the geomorphological maps of the conduits projected below the main passages of the cavity.

Fig. 3. Profile of the pilot caves indicating the position of the recognized cave levels: (a) Torca Teyera, (b) Torca La Texa, (c) El Frailín de Camplengu, (d) Pozu Lluçia.

Fig. 4. (a) Vadose canyon incised by a cave stream. The canyon shows thalweg deposits partially covered by a rich-detrital flowstone eroded by the stream. (b) Phreatic/epiphreatic conduits with dissolution pockets and pendants. (c) Breakdown-modified passages with debris from ceiling collapses and flowstone affected by collapses (picture courtesy of S. Ferreras).

Fig. 5. (a) Fluvial terrace deposits of the Torca Teyera cave perched 9 m above a cave stream, showing an interbedded flowstone. (b) Fluvial terrace deposit of Torca Teyera. (c) Fluvial deposit terrace covered by a flowstone preserved at a wall of the Pozu Lluçia shaft.

Fig. 6. (a) A ledge of flowstone of El Frailín de Camplengu. (b) Sample of the ledge of a flowstone precipitated above fluvial sediments.

Fig. 7. Cave sections sketches depicting the geomorphological setting of the new 28 speleothems dated by U/Th, as well as the six previous dates performed in the pilot caves (sub-sections from f to k) (Ballesteros et al., 2015a, 2017). The sub-sections (b), (e), (f), (h), (s), (t) and (ab) provide the reference ages for the fluvial deposition while the sub-sections (n), (o), (r) and (u) support the reference timing for the breakdown processes.

Fig. 8. U/Th dates grouped in four generations (in grey) according to their ages. Erosive scars recognised in some dated speleothem indicate the incision of the cave streams after the speleothem precipitation.

Fig. 9. Geomorphological map of the study area defined in Fig. 1c. Speleological groups detailed in the acknowledgements provided the cave conduits information displayed in the map.

Fig. 10. Field evidence of relationship between caves and younger erosive landforms: (a) Border polje of Vega de Comeya (N of the study area; Fig. 9) cutting the Infiernu Cave (~4 km length) and other phreatic/epiphreatic conduits. (b) The vadose shaft of Pozu Los Texas (240 m depth) decapitated by glaciers. (c) The karst spring of the Humhumia River probably blocked by glaciers in the past. (d) Doline intercepting a phreatic/epiphreatic conduit with 169 m length.

Fig. 11. Conceptual model based on transversal sections of the pilot caves conduits depicting their temporal evolution according to the proposed speleogenetic model. The phreatic/epiphreatic conduits originated in phase 1 evolved following three paths: (a) almost without changes; (b and c) as dominated by fluvial incision that generated narrow (b) or wide vadose canyons (c); and (d) as vadose canyons that developed independently after phase 2.

Fig. 12. Configuration of the relief during the six speleogenetic phases from a point view located to the NW (X: 340 Y: 4800 Z: 8 km). (a) Phase 1 showing the Permian-Mesozoic cover above the karst (Smart, 1986; Fernández-Gibert et al., 2000). (b) Phase 2 with a partially eroded Alpine sedimentary cover and Carboniferous Stephanian outcrops larger than nowadays. (c) Phase 3 under the possible influence of glaciers during the MIS6-7. (d) Phase 4 coeval with the local glacial maximum extension that took place during the MIS5-4. (e) Phase 5 showing glaciers occupying the highest areas of the Western Massif, while the Enol lake was collecting glacial

melting water during the MIS 2 (Moreno et al., 2010). (f) Phase 6 with glaciers occupying the El Brial depression and without connection to the Enol Lake (MIS 1). (g) Phase 6 during the cirque glacier stage. (h) Orthophotography 2007 of the Western Massif projected above the Digital Elevation Model used to reconstruct the landscape.

Table 1. Dimensions, type of conduits and cave levels of the studied caves.

Cave	Torca Teyera	Torca La Texa	El Frailín de Camplengu	Pozu Lluçia	Total caves	
Altitude of the entrance (m)	1335	1305	1331	1266		
Length (km)	4.4	2.6	2.7	2.3	12.0	
Depth (m)	738	215	245	244		
Type of conduits (% of the cave length)	vadose canyons and shafts	55	51	49	51	47
	Phreatic/epiphreatic conduits	38	43	41	48	45
	Breakdown-modified passages	7	5	9	7	7
Cave levels (m a.s.l.)	1	1300				
	2		1238-1273	1275	1240	
	3		1168	1179	1163-1173	
	4			1075	1083	
	5	700-800				
	6	615				

Table 2. Results of 28 new $^{234}\text{U}/^{230}\text{Th}$ datations by alpha-spectrometry. We applied the isochron method to calculate the age of the samples FR-03, FR-17, FR-18, LL-22 and LL-23. Cave levels are detailed in Table 1.

Sample	Speleothem	Cave level	Lab. Ref.	^{238}U (ppm)	^{232}Th (ppm)	$^{234}\text{U}/^{238}\text{U}$	$^{230}\text{Th}/^{232}\text{Th}$	$^{230}\text{Th}/^{234}\text{U}$	Nominal date (a BP)	Isochron date (a BP)
Torca Teyera										
TEY-01	Flowstone	5	5309	0.04	0.07	1.16 ± 0.07	2.145 ± 0.127	0.92 ± 0.05	238083 +56456/-37939	
TEY-02	Flowstone	5	5109	0.12	0.15	1.33 ± 0.05	2.873 ± 0.129	0.86 ± 0.04	185344 +20293/-17385	
TEY-03	Flowstone	5	5209	0.11	0.43	1.09 ± 0.05	0.875 ± 0.030	1.05 ± 0.05	> 300000	
TEY-04	Pool deposit	1	1210 1	0.42	1.17	1.93 ± 0.03	2.506 ± 0.062	1.15 ± 0.04	> 300000	
Torca La Texa										
TEX-26	Stalagmite	2	3413	6.68	<0.00	4.30 ± 0.04	-	0.01 ± 0.00	1330 +94/-94	
TEX-29	Flowstone	2	6814	0.06	0.02	2.83 ± 0.16	2.851 ± 0.320	0.12 ± 0.01	13304 +974/-967	
El Frailín de Camplengu										
FR-03	Flowstone	2	714	0.26	0.58	0.86 ± 0.02	2.889 ± 0.117	2.38 ± 0.10	>350000	
FR-03 (lix)	Flowstone	2	814	0.14	0.31	1.43 ± 0.04	4.306 ± 0.145	2.11 ± 0.07	>350000	
FR-03 (res)	Flowstone	2	1314	4.07	10.39	0.64 ± 0.03	0.711 ± 0.060	0.92 ± 0.08	>350000	>350000
FR-09	Flowstone	2	2014	0.10	<0.00	2.58 ± 0.10	-	0.65 ± 0.03	99603 +6386/-6103	
FR-10	Flowstone	2	1415	0.24	0.22	1.52 ± 0.04	5.390 ± 0.159	1.08 ± 0.03	>350000	
FR-11	Stalagmite	3	515	0.16	0.03	3.14 ± 0.08	43.688 ± 3.134	0.93 ± 0.03	181842 +10525/-9808	
FR-12	Stalagmite	2	1815	0.05	<0.00	2.33 ± 0.13	-	0.74 ± 0.04	124239 +10367/-9636	
FR-13	Stalagmite	2	1515	0.55	0.01	1.00 ± 0.02	139.715 ± 15.02	0.94 ± 0.03	300027 +55541/-36665	
FR-14	Stalagmite	2	2015	0.30	0.03	1.05 ± 0.02	29.894 ± 2.535	0.088 ± 0.03	218540 +21695/-18174	
FR-15	Flowstone	2	815	0.11	0.11	1.91 ± 0.06	5.764 ± 0.338	0.95 ± 0.04	205453 +19991/-17410	
FR-16	Flowstone	2	2715	0.12	0.04	1.55 ± 0.05	13.985 ± 0.768	1.03 ± 0.03	286614 +40873/-30732	
FR-17 (A)	Flowstone	1	915	0.25	0.38	0.92 ± 0.02	1.857 ± 0.119	0.98 ± 0.05	>350000	
FR-17 (B)	Flowstone	1	2315	0.25	0.44	0.95 ± 0.03	1.610 ± 0.040	0.95 ± 0.04	>350000	>350000
FR-18	Flowstone	1	1015	0.55	0.75	0.88 ± 0.01	1.740 ± 0.045	0.87 ± 0.03	258021 +47355/-31960	
FR-18 (lix)	Flowstone	1	2415	0.30	0.41	1.21 ± 0.02	2.416 ± 0.058	0.88 ± 0.02	205455 +15868/-14002	192327 +52158/-37834
Pozu Lluçia										
LL-04	Flowstone	1	1614	0.13	0.17	2.18 ± 0.07	0.818 ± 0.052	0.16 ± 0.01	+18633 1123/-1113	
LL-13	Stalactite	2	6914	0.36	<0.00	2.14 ± 0.05	-	0.54 ± 0.02	77525 +3277/-3199	
LL-14	Flowstone	2	1115	0.39	0.08	1.84 ± 0.03	2.437 ± 0.127	0.09 ± 0.00	9783 +376/-375	
LL-15	Flowstone	2	2215	0.07	0.02	1.12 ± 0.05	9.177 ± 0.866	0.70 ± 0.03	126100 +11388/-10357	
LL-17	Stalagmite	3	715	0.05	0.03	2.53 ± 0.14	10.918 ± 0.854	0.72 ± 0.03	116349 +8278/-7810	
LL-18	Stalagmite	3	415	0.05	<0.00	3.08 ± 0.14	-	0.10 ± 0.01	11723 +967/-960	

LL-20	Stalagmite	2	1615	0.03	<0.00	1.45 ± 0.10	-	0.99 ± 0.06	258666 +72647/-46125	
LL-21	Flowstone	2	615	0.04	0.02	3.59 ± 0.18	12.742 ± 1.261	0.47 ± 0.02	63194 +3403/-3324	
LL-22 (A)	Flowstone	2	1315	0.03	0.01	3.17 ± 0.18	4.123 ± 0.569	0.16 ± 0.01	18780 +1426/-1412	
LL-22 (B)	Flowstone	2	2515	0.02	0.01	3.59 ± 0.23	3.302 ± 0.435	0.16 ± 0.01	18166 +1426/-1411	21751 +2402/- 2358
LL-23 (A)	Stalagmite	2	1215	0.04	0.06	2.84 ± 0.14	1.763 ± 0.147	0.29 ± 0.02	35760 +2522/-2477	
LL-23 (B)	Stalagmite	2	2615	0.06	0.11	2.60 ± 0.11	1.571 ± 0.073	0.40 ± 0.02	53465 +2730/-2677	9710 +1014/ 1007
LL-24	Flowstone	2	1715	0.07	<0.00	1.67 ± 0.07	-	0.34 ± 0.02	44588 +2660/-2605	

Table 3. ^{26}Al and ^{10}Be concentrations, the burial age and erosion rate estimated for a fluvial deposit of cave level 5 in the Torca Teyera cave.

Sample	^{26}Al (10^6 at/g)	^{10}Be (10^6 at/g)	$^{26}\text{Al}/^{10}\text{Al}$	Burial age (Ma)	Erosion rate (mm a^{-1})
TEY-05	617897 ± 155583	256538 ± 13134	2.409 ± 0.619	2.108 ± 0.484	0.012 ± 0.001

Table 4. Uplifting rates estimated by geomorphology and thermochronology methods in the Cantabrian Mountains and Coast.

Indicator	Place	Uplifting rate (mm·a ⁻¹)	Temporal range	Reference
Fluvial terraces of the Cares River in Arenas de Cabrales	N of Picos de Europa	0.24	37 ka	Ruiz-Fernández and Poblete Piedrabuena (2011)
Phreatic conduits of Cueva del Agua and other cavities	Eastern Massif of Picos de Europa	0.3	350 ka	Smart (1984)
Phreatic conduits of El Pindal cave	Central Cantabrian Coast	0.19	200 ka	Jiménez-Sánchez et al. (2006)
Fluvial terraces of Miño River	Western Cantabrian Mountains	0.1	600 ka	Viveen et al. (2014)
Cave levels of El Soplao Cave	Central Cantabrian Mountains	0.125-0.213	1.5 Ma	Rossi et al. (2016)
Marine terraces	Western Cantabrian Coast	0.07-0.1	1-2 Ma	Alvarez-Marrón et al. (2008)
Apatite thermochronology	Western Cantabrian Mountains	0.06	Neogene-Quaternary	Martín-González et al. (2011)
Apatite and He thermochronology	Western Cantabrian Mountains	0.00025	Upper Jurassic-Quaternary	Grobe et al. (2014)

Highlights

A regional landscape evolution based on cave geomorphology and geochronology.

Cave levels and subsequent vadose incision were formed at least Middle Pleistocene.

Cave sedimentary infill likely occurred at 220-145 ka from detrital rock erosion.

Cave infill was probably eroded at 125-45 ka.

Ancient presence of detrital rocks at the surface controlled the speleogenesis

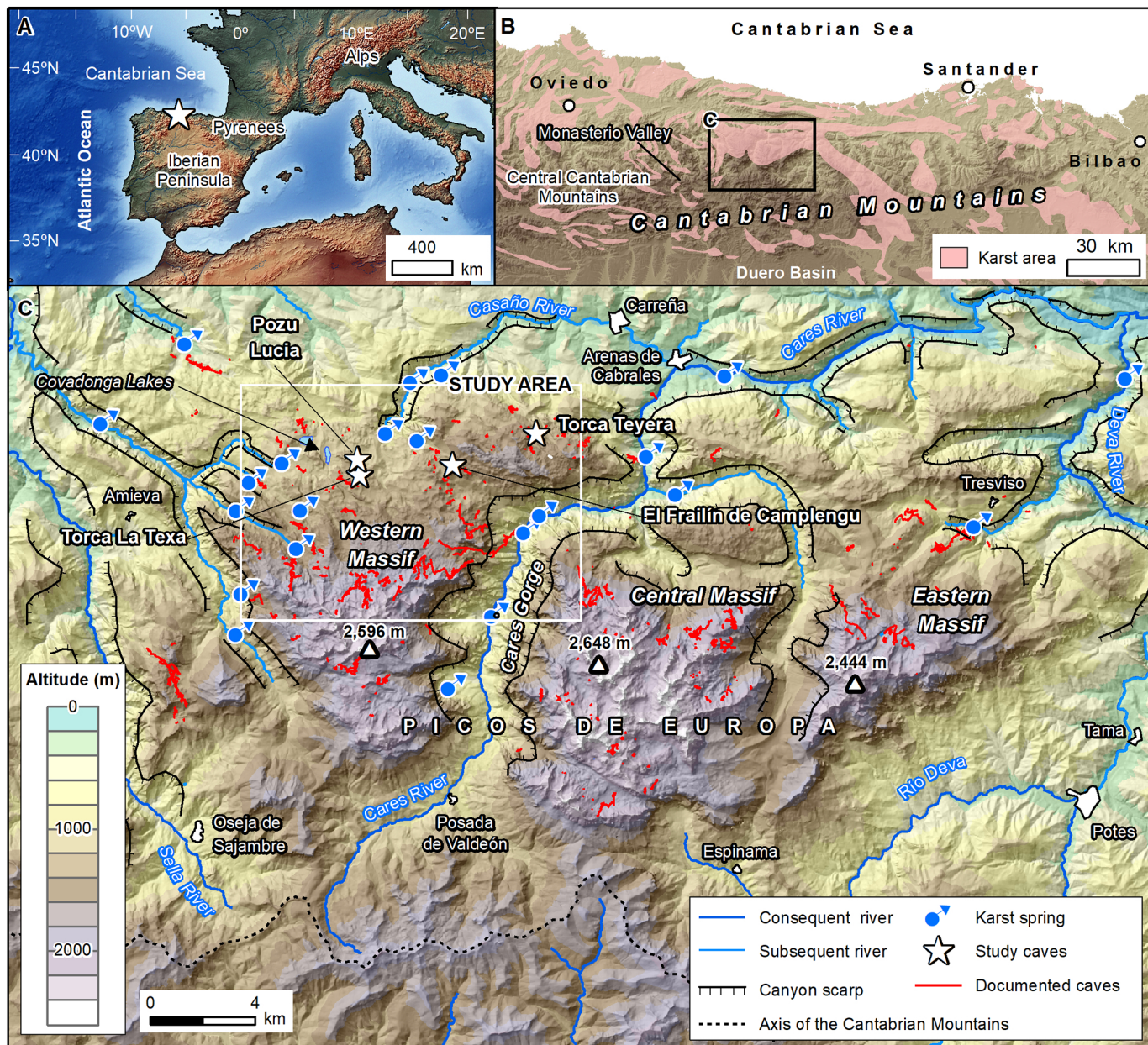


Figure 1

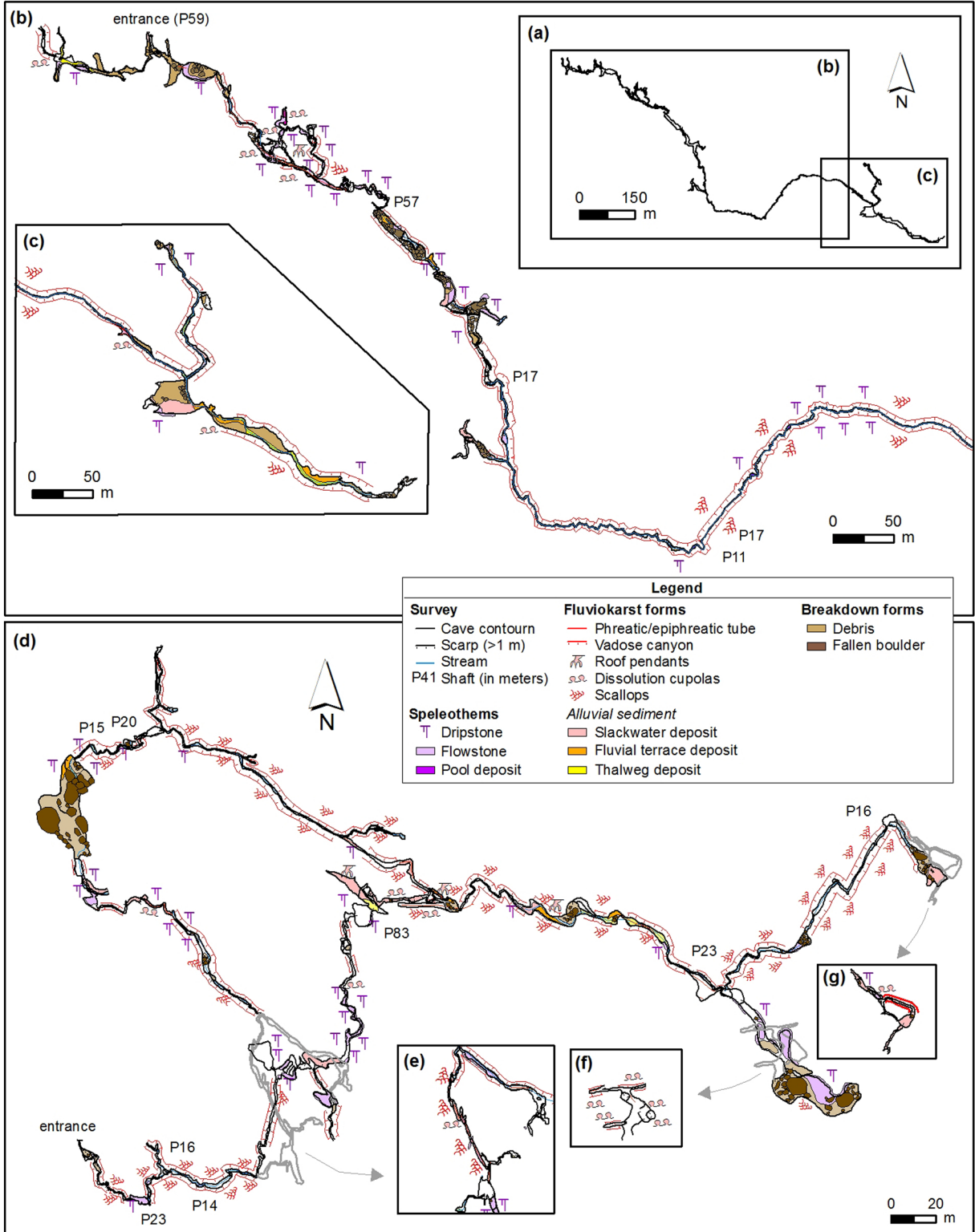


Figure 2

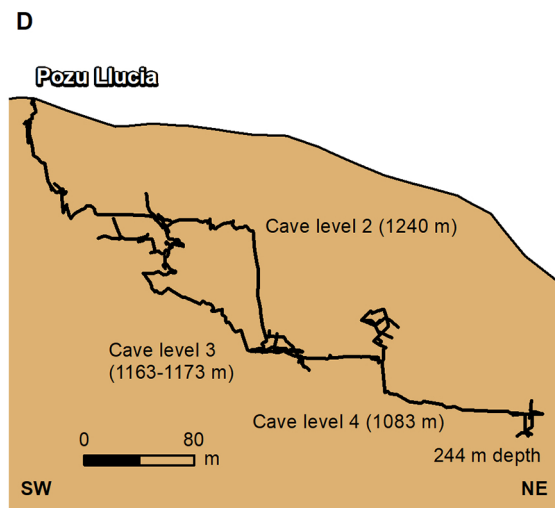
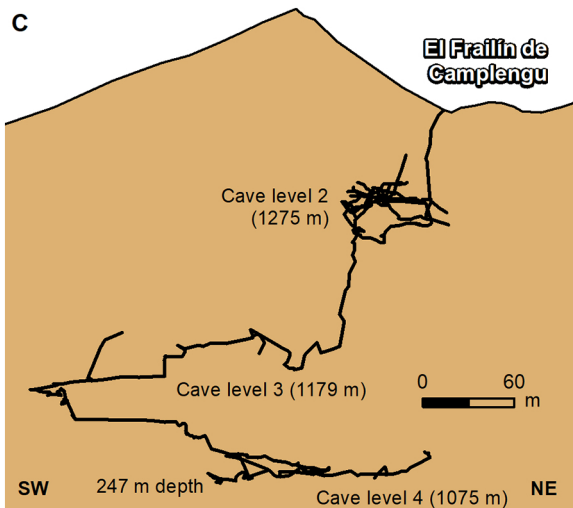
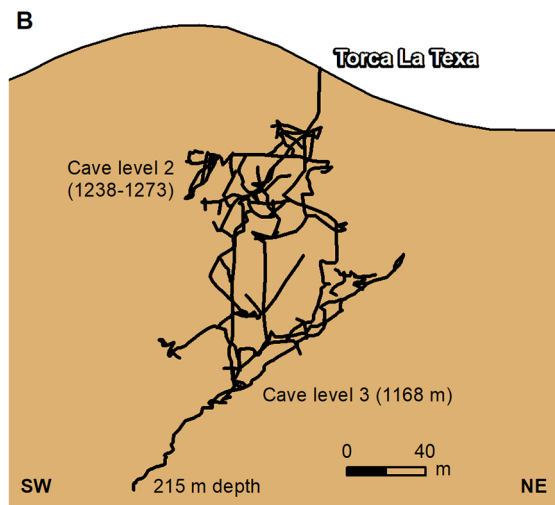
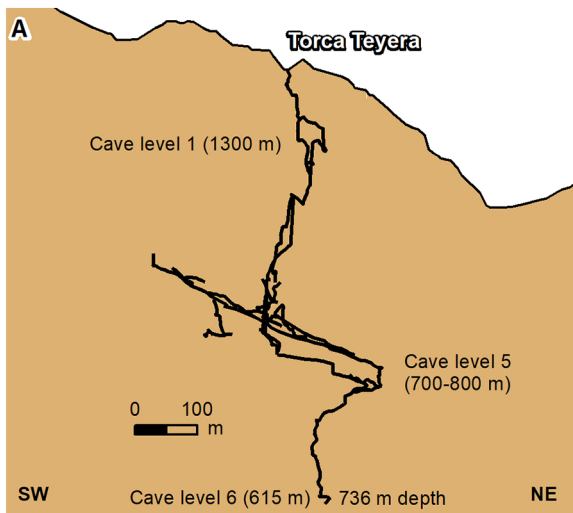


Figure 3

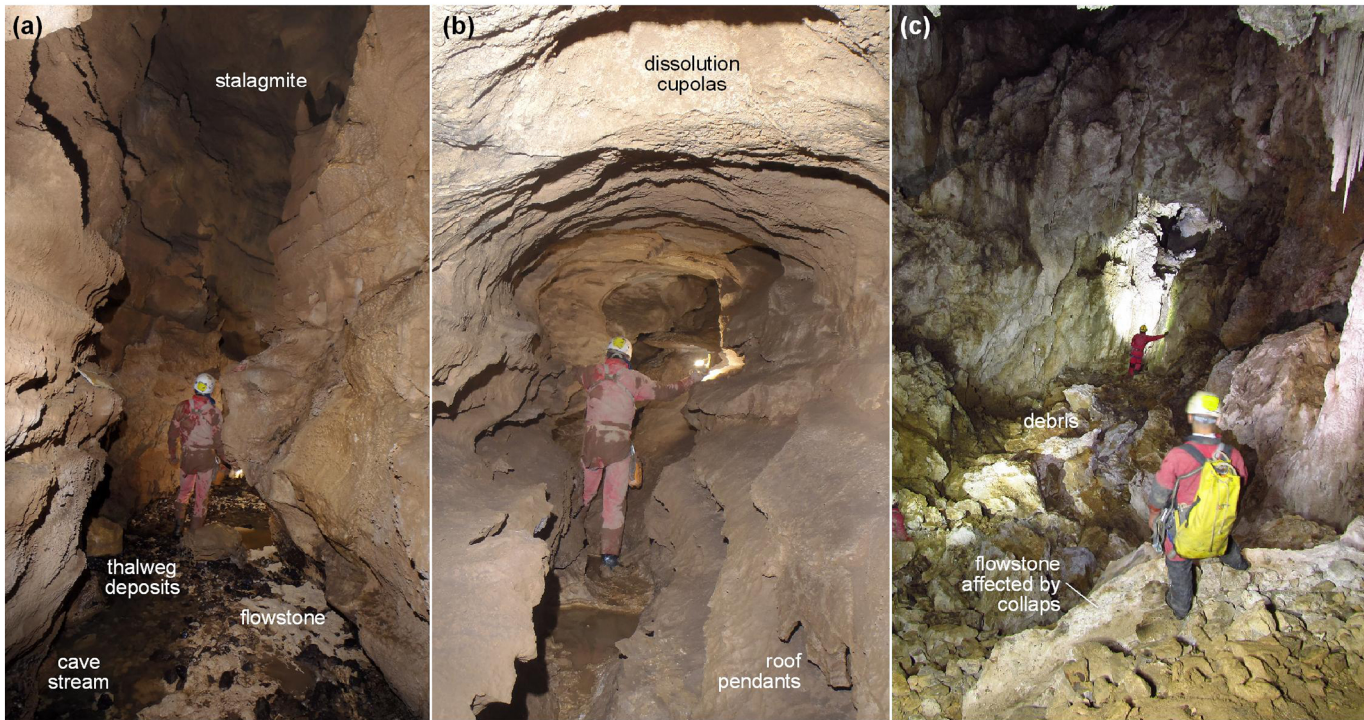


Figure 4

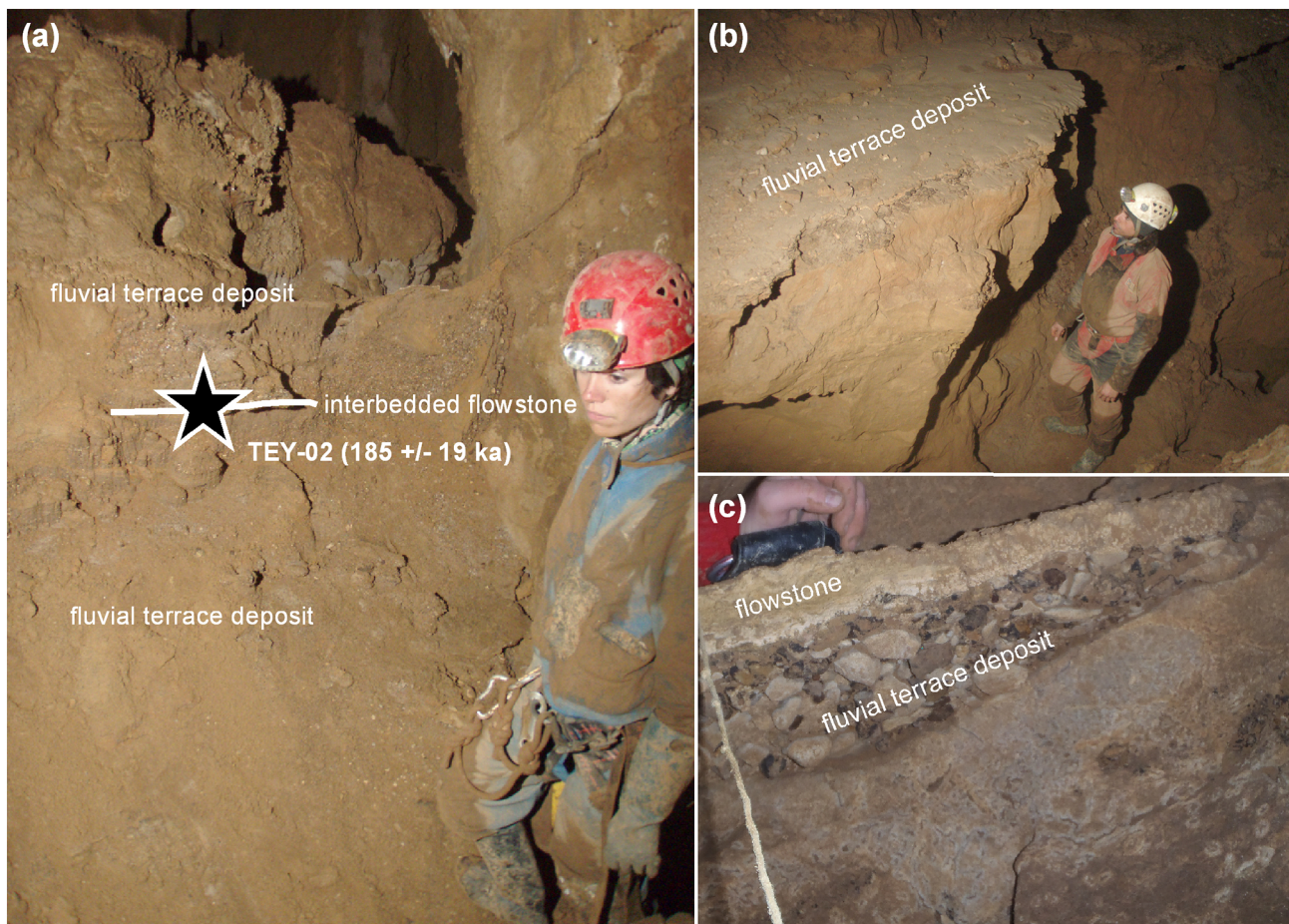


Figure 5

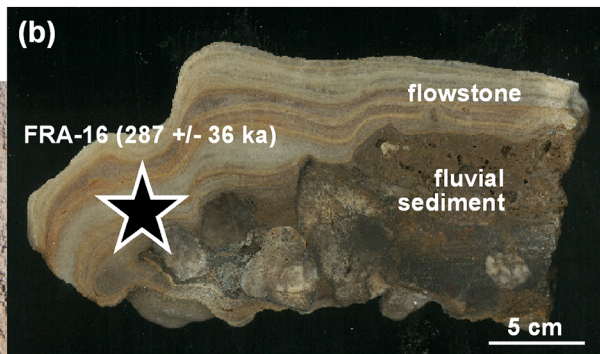
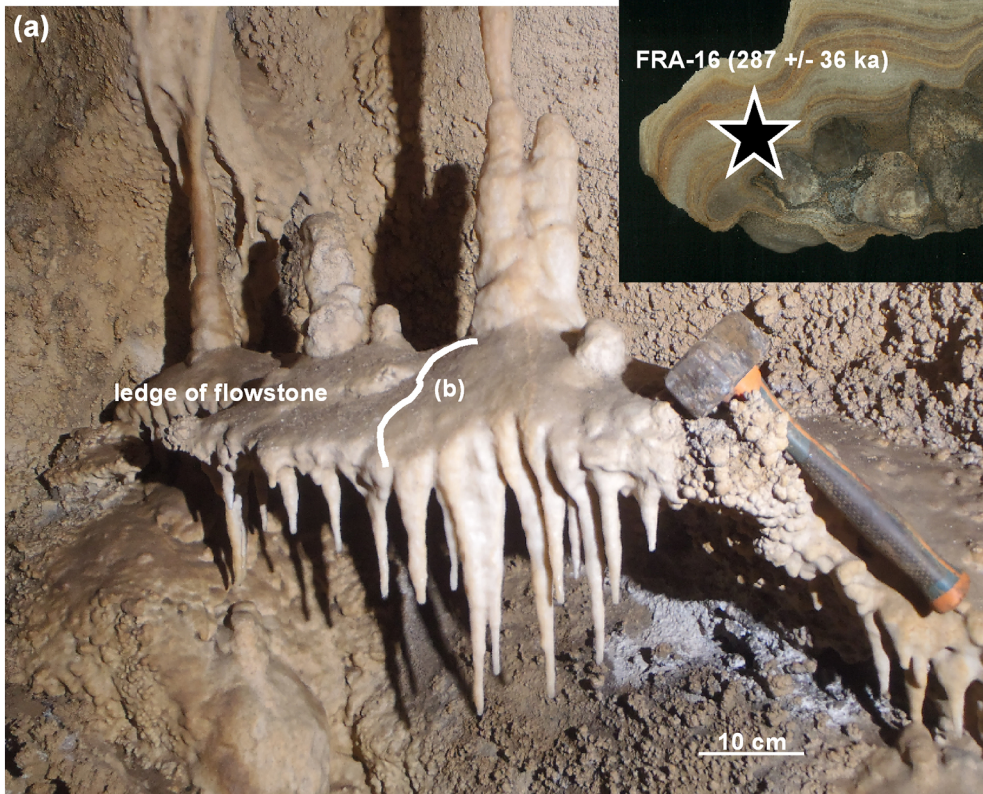


Figure 6

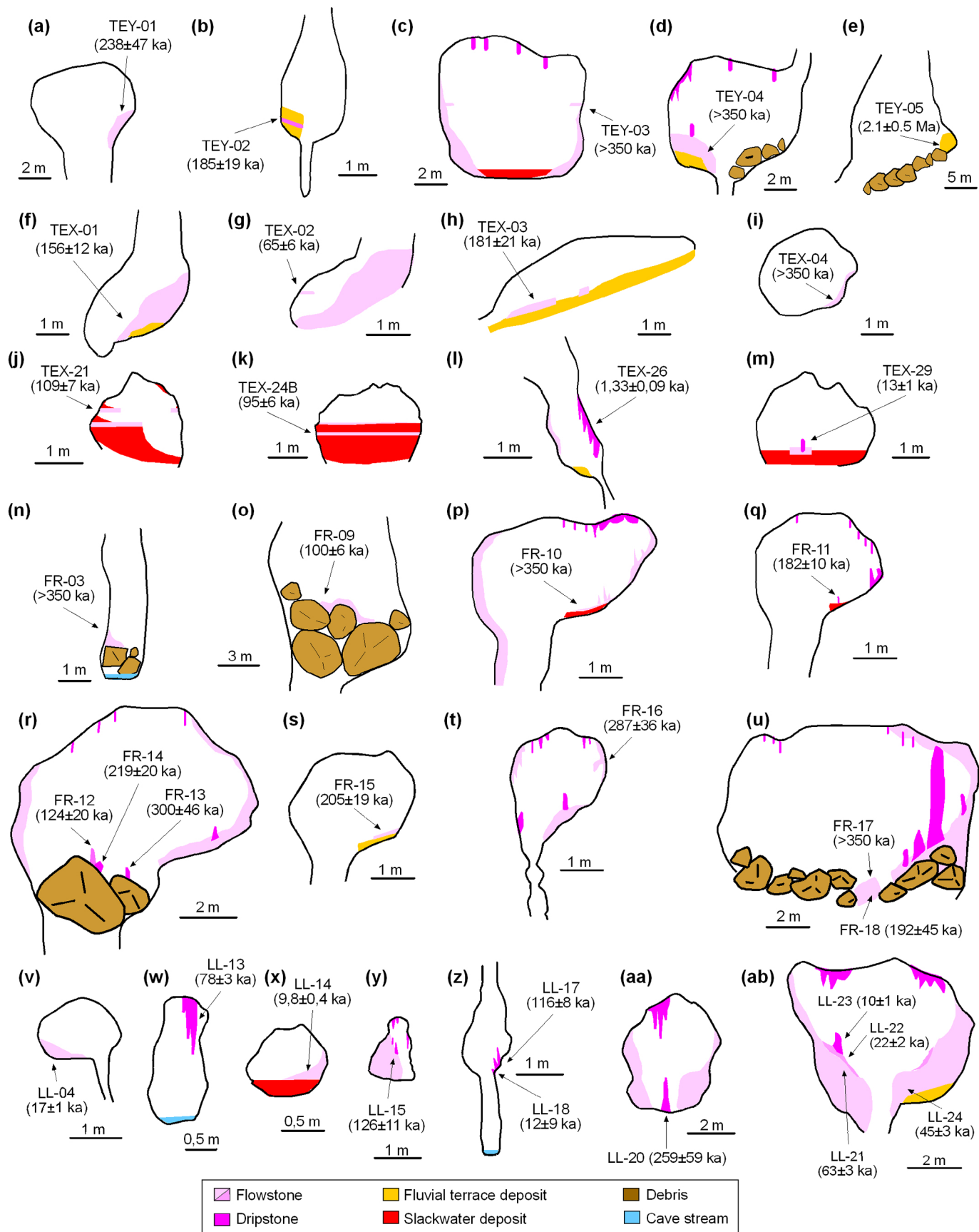


Figure 7

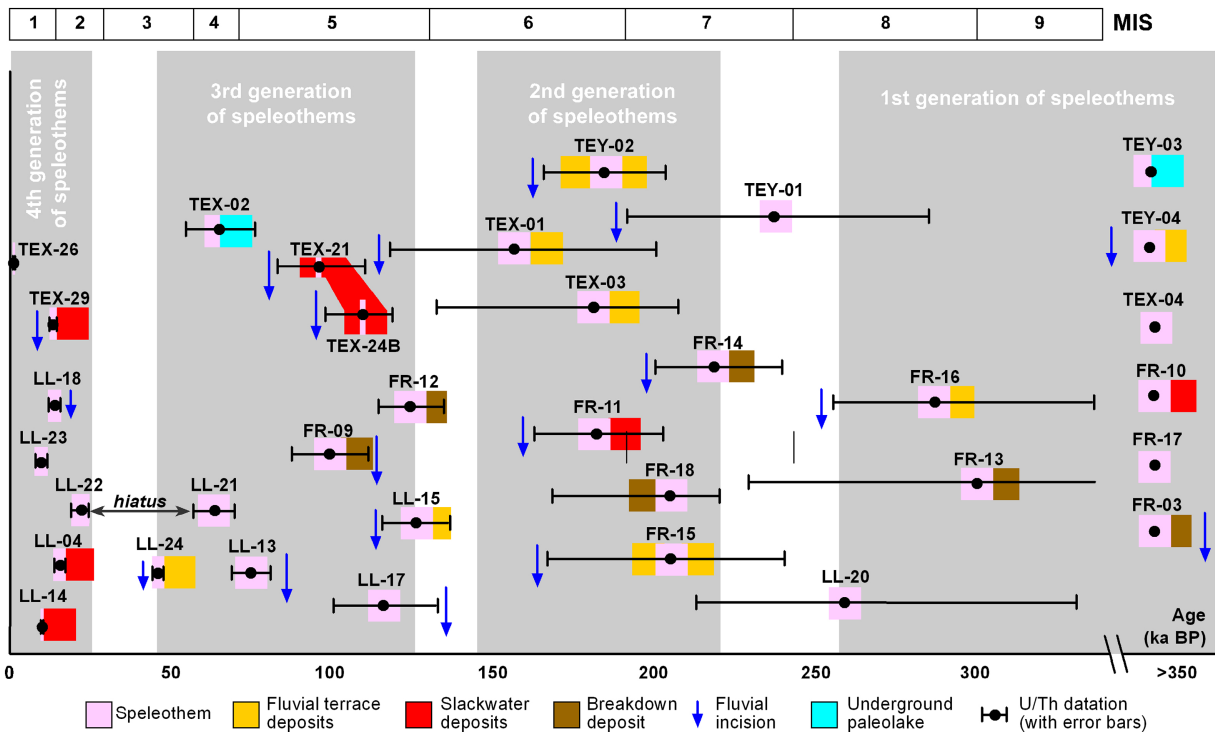


Figure 8

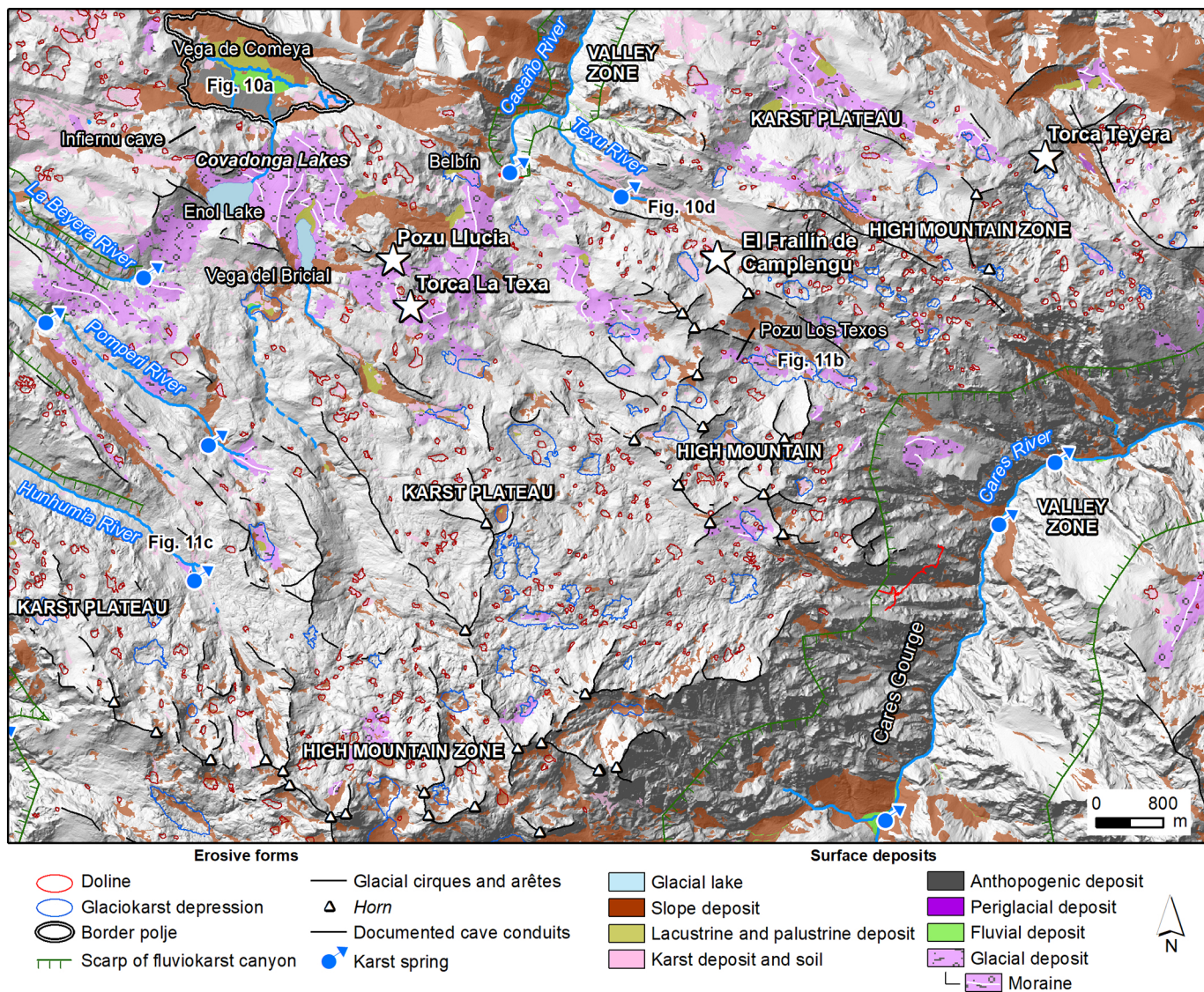


Figure 9



Figure 10

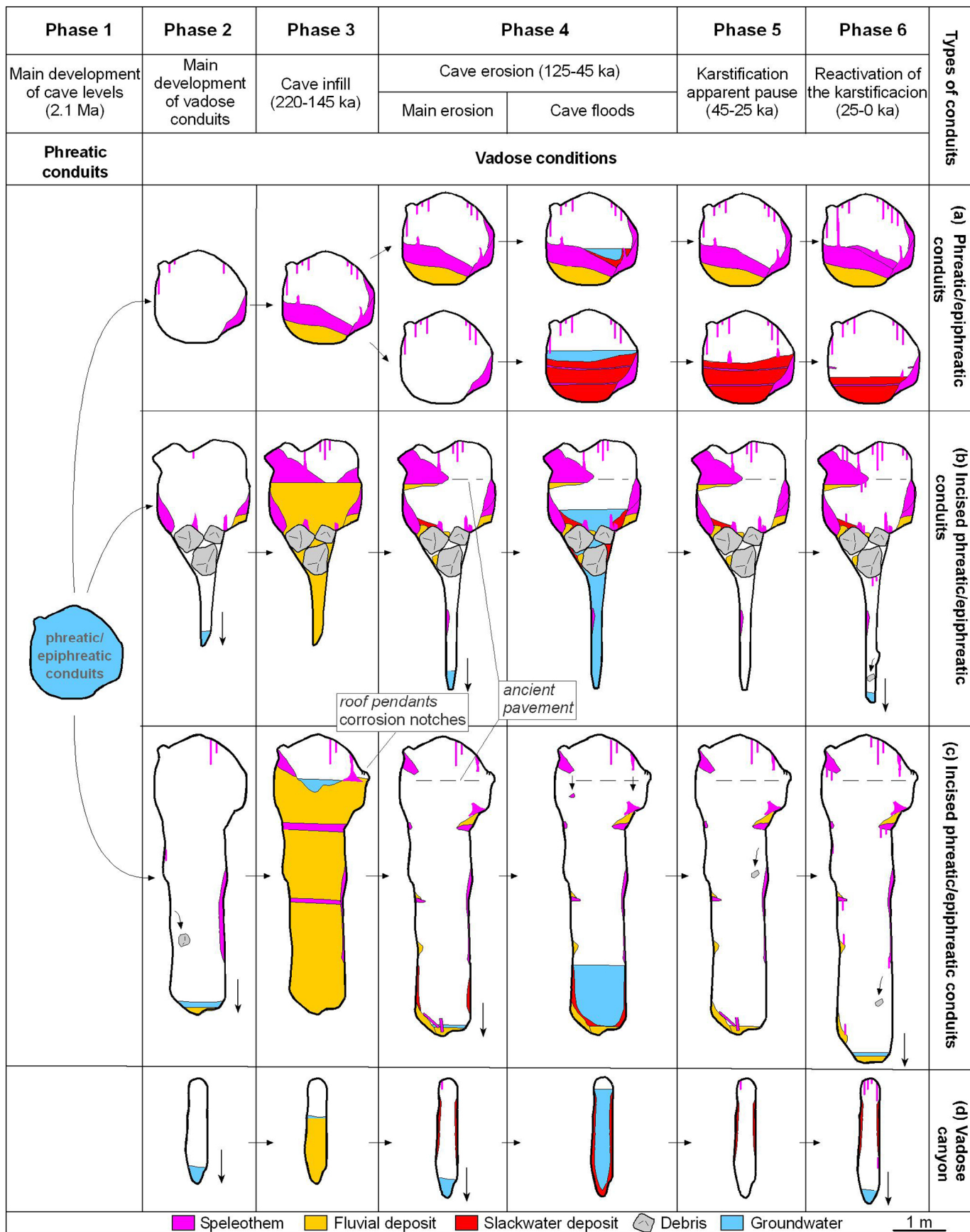


Figure 11

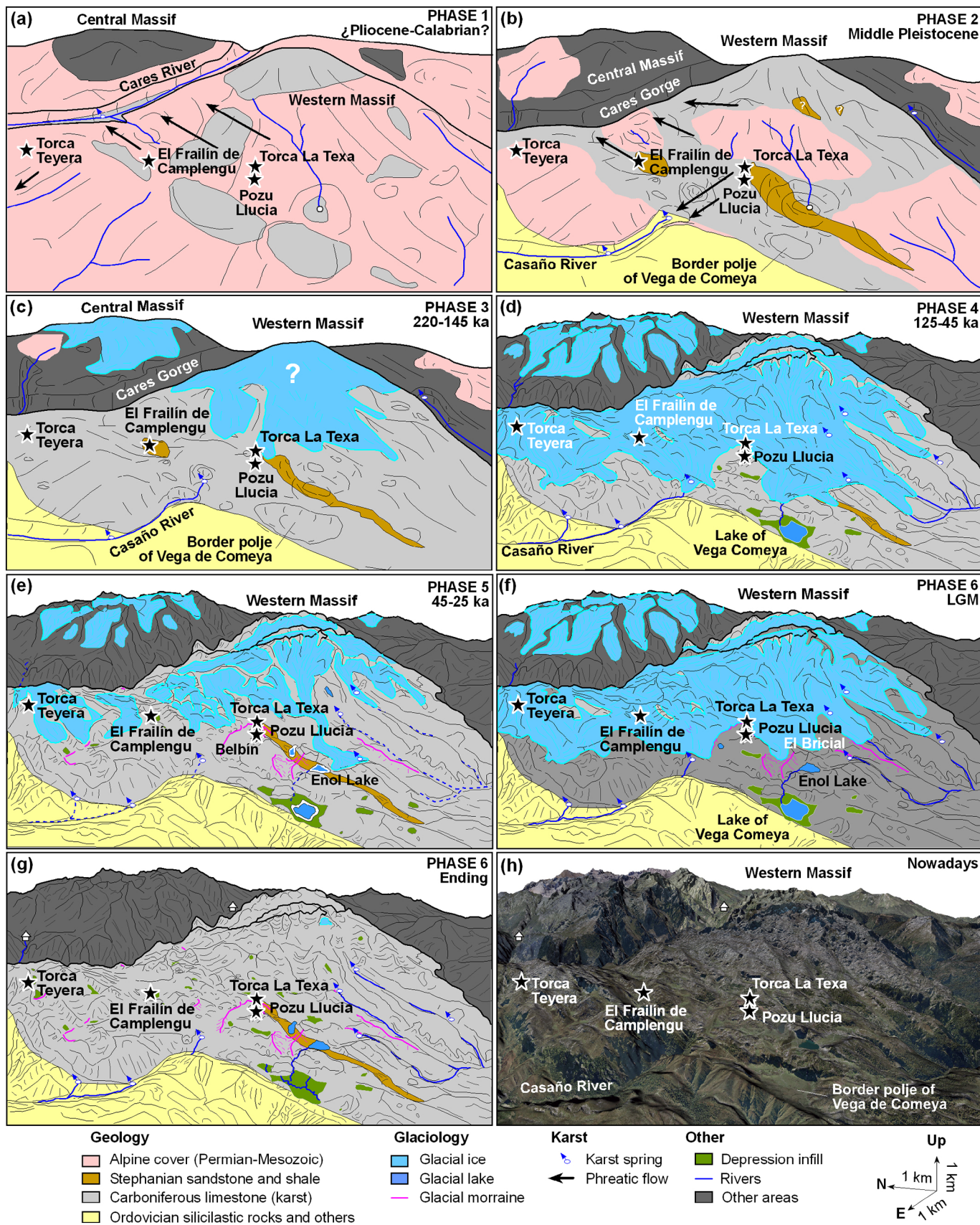


Figure 12